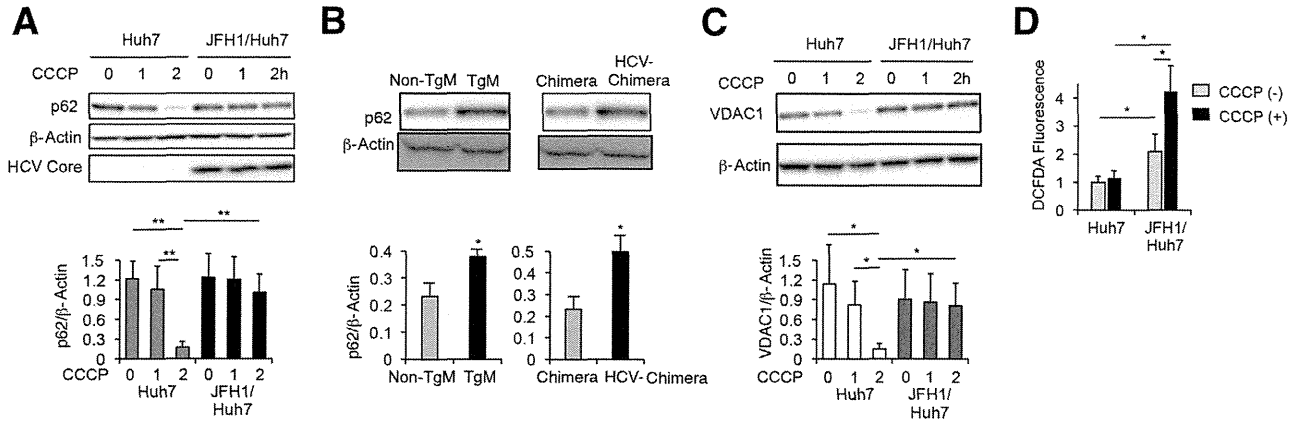

Figure 9 Effect of HCV infection on cellular p62 and VDAC1 expression after carbonyl cyanide *m*-chlorophenylhydrazone (CCCP) treatment and reactive oxygen species (ROS) production. **A:** Immunoblots for p62 using whole cell lysates of Huh7 and JFH1-Huh7 cells before and after a 1- and a 2-hour CCCP treatment ($n = 5$). **B:** Immunoblots for p62 using the liver from non-transgenic (non-TgM) and TgM ($n = 5$) mice and from chimeric mice without or with HCV infection ($n = 5$). The p62 expression level was normalized to β-actin. **C:** Immunoblots for VDAC1 using whole cell lysates of Huh7 and JFH1-Huh7 cells before and after a 1- and a 2-hour CCCP treatment ($n = 5$). The VDAC1 expression level was normalized to β-actin. **D:** Changes in cellular ROS production after a 1-hour CCCP treatment in Huh7 and JFH1-Huh7 cells ($n = 5$). $^{*}P < 0.05$, $^{**}P < 0.01$.

JFH1-Huh7 cells than in Huh7 cells (Figure 8D). These results were consistent with a previous study that showed an essential role of mitophagy in reducing mitochondrial ROS production[40] and, therefore, may reflect the suppressed mitophagy in the presence of HCV infection.

Discussion

Mitophagy may likely be induced in HCV-JFH1–infected cells in the context of mitochondrial depolarization, and in transgenic mice expressing the HCV polyprotein or in HCV-infected chimeric mice, both of which showed the decreased mitochondrial GSH content. Our results suggest that the HCV core protein inhibits mitophagy during HCV infection and that the molecular mechanisms by which this suppression occurs include the interaction of the HCV core protein with Parkin and the inhibition of Parkin translocation to the mitochondria. This inhibition leads to the failure of mitochondrial ubiquitination, mitophagosome formation, and autophagic degradation (Figure 10). Because Parkin 1 to 215 contains one of the critical amino acids required for mitochondrial localization, the specific interaction of Parkin 1 to 215 with the HCV core protein strongly suggests that the core protein represses mitophagy by inhibiting Parkin translocation to the mitochondria. We know that PINK1 accumulates in the mitochondria and phosphorylates Parkin after CCCP treatment and that the suppression of the mitochondrial Parkin signal occurs by blocking PINK1 via siRNA. Therefore, we could exclude the possibility that PINK1 plays a role in suppressing the recruitment of Parkin to the mitochondria. To our knowledge, this is the first report to demonstrate a suppressive effect of a viral protein on mitophagy via an interaction with Parkin. Interestingly, silencing Parkin via siRNA inhibited HCV core expression, which was consistent with the results of a recent study.[28] These results suggest that HCV potentially uses Parkin for its replication through the interaction between the HCV core protein and Parkin. Parkin may be post-transcriptionally involved in HCV replication, because Parkin silencing did not affect HCV core mRNA levels.

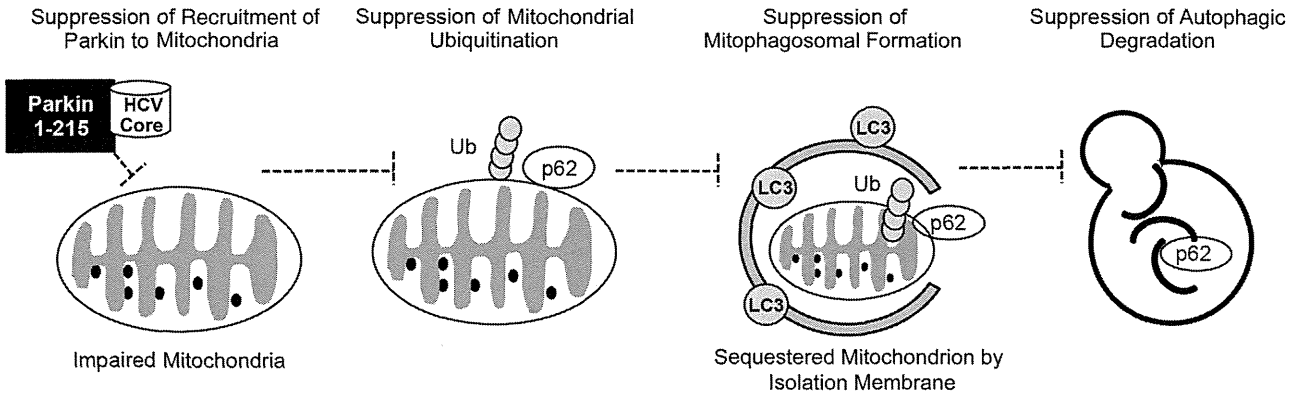

Figure 10 A schematic diagram depicting the mechanisms underlying mitophagy suppression by the HCV core protein. The HCV core protein interacts with the Parkin N-terminal fragment containing the RINGO domain (designated Parkin 1 to 215) and inhibits Parkin translocation to the mitochondria, which leads to the failure of mitochondrial ubiquitination, autophagosome formation, and autophagic degradation. Ub, ubiquitin.

Further studies are required to clarify the mechanisms underlying this speculation.

Two types of autophagy have been identified: nonselective and selective. For nonselective autophagy related to HCV infection, previous studies have reported the enhanced accumulation of autophagosomes without any effect on autophagic protein degradation,[33] the requirement of LC3 for efficient HCV replication,[34] and the occurrence of HCV RNA replication on autophagosomal membranes.[36] Mitophagy is selective and is induced by mitochondrial membrane depolarization, followed by Parkin recruitment to the mitochondria.[9–15] Herein, mitophagosome accumulation was suppressed because of mitophagy inhibition, whereas HCV infection enhanced the expression of LC3-II and autophagosome accumulation under nonselective autophagy-inducible conditions. Therefore, the present results are consistent with the previously characterized HCV-induced nonselective autophagic response.[34,35,38] However, a recent report has shown that HCV induces the mitochondrial translocation of Parkin and subsequent mitophagy,[28] which contrasts with the present results, except for the inhibitory effect of Parkin silencing on HCV replication. One of the significant differences in the method between the two studies was the presence or absence of CCCP treatment. Whether HCV-induced mitophagy was preceded by mitochondrial depolarization was unknown because $\Delta\Psi$ was not measured in the previous report of HCV-induced mitophagy.[28] However, we need to be careful that the mitochondrial depolarization by CCCP treatment is not a pathophysiological condition observed in HCV infection and that CCCP causes the depolarization of the entire mitochondrial network.[41] It is currently unknown whether CCCP treatment caused paradoxical results on mitophagy in HCV-infected cells between our study and a previous one.[28] Although suppressed mitophagy was also found in FL-N/35-transgenic mice and HCV-infected chimeric mice without any treatment, these mice may not be simply compared with HCV-JFH1–infected cells in terms of extremely low levels of viral proteins in FL-N/35-transgenic mice or spontaneous oxidized mitochondrial glutathione in both mice. Another difference between two studies was postinfection time from infection to assessment of mitophagy in HCV-JFH1–infected cells (21 versus 3 days). However, further studies are required to clarify whether postinfection time of HCV-JFH1–infected cells affects the interaction of HCV with Parkin. Oxidative stress and/or hepatocellular mitochondrial alterations are present in chronic hepatitis C to a greater degree than in other inflammatory liver diseases,[1,6] and mitophagy is important for maintaining mitochondrial quality by eliminating damaged mitochondria. Therefore, our results that the HCV core protein suppresses mitophagy appear reasonable in the context of what is known about the pathophysiological characteristics of chronic hepatitis C.

HCV-induced mitochondrial injury, ROS production, and subsequent oxidative stress contribute to HCC development in FL-N/35-transgenic mice that receive modest iron supplementation.[8] The relatively long period (12 months) required for HCC development suggests that mitochondrial injury, as a source of oxidative stress, must continue for a prolonged period. Mitochondrial DNA mutations are also relevant to HCC development in patients with chronic HCV infections.[42] Indeed, mitophagy plays an essential role in reducing mitochondrial ROS production and mitochondrial DNA mutations in yeast[40] and eliminating oxidative damaged mitochondria.[43] In addition to the directly induced generation of ROS by HCV proteins, the suppression of mitophagy by the HCV core protein has the potential to generate an additional long-lasting ROS burden and may offset or overwhelm the physiological antioxidative activity in mitochondria. Therefore, the suppressive effect of the HCV core protein on mitophagy may be an important mechanism of HCV-induced hepatocarcinogenesis.

In conclusion, results indicate that HCV core protein suppresses mitophagy by inhibiting Parkin translocation to the mitochondria via a direct interaction with Parkin in the context of mitochondrial depolarization. These findings have implications for the amplification and sustainability of mitochondria-induced oxidative stress observed in patients with HCV-related chronic liver disease and an increased risk of hepatocarcinogenesis.

Acknowledgments

We thank Dr. Stanley M. Lemon for the transgenic mice, Dr. Takaji Wakita for the JFH1 clone, and Hikari Hara for technical assistance.

References

1. Farinati F, Cardin R, De Maria N, Della Libera G, Marafin C, Lecis E, Burra P, Floreani A, Cecchetto A, Naccarato R: Iron storage, lipid peroxidation and glutathione turnover in chronic anti-HCV positive hepatitis. J Hepatol 1995, 22:449–456
2. Valgimigli M, Valgimigli L, Trere D, Gaiani S, Pedulli GF, Gramantieri L, Bolondi L: Oxidative stress EPR measurement in human liver by radical-probe technique: correlation with etiology, histology and cell proliferation. Free Radic Res 2002, 36:939–948
3. Okuda M, Li K, Beard MR, Showalter LA, Scholle F, Lemon SM, Weinman SA: Mitochondrial injury, oxidative stress, and antioxidant gene expression are induced by hepatitis C virus core protein. Gastroenterology 2002, 122:366–375
4. Moriya K, Nakagawa K, Santa T, Shintani Y, Fujie H, Miyoshi H, Tsutsumi T, Miyazawa T, Ishibashi K, Horie T, Imai K, Todoroki T, Kimura S, Koike K: Oxidative stress in the absence of inflammation in a mouse model for hepatitis C virus-associated hepatocarcinogenesis. Cancer Res 2001, 61:4365–4370
5. Korenaga M, Wang T, Li Y, Showalter LA, Chan T, Sun J, Weinman SA: Hepatitis C virus core protein inhibits mitochondrial electron transport and increases reactive oxygen species (ROS) production. J Biol Chem 2005, 280:37481–37488
6. Barbaro G, Di Lorenzo G, Asti A, Ribersani M, Belloni G, Grisorio B, Filice G, Barbarini G: Hepatocellular mitochondrial alterations in patients with chronic hepatitis C: ultrastructural and biochemical findings. Am J Gastroenterol 1999, 94:2198–2205

7. Nishina S, Hino K, Korenaga M, Vecchi C, Pietrangelo A, Mizukami Y, Furutani T, Sakai A, Okuda M, Hidaka I, Okita K, Sakaida I: Hepatitis C virus-induced reactive oxygen species raise hepatic iron level in mice by reducing hepcidin transcription. Gastroenterology 2008, 134:226–238
8. Furutani T, Hino K, Okuda M, Gondo T, Nishina S, Kitase A, Korenaga M, Xiao SY, Weinman SA, Lemon SM, Sakaida I, Okita K: Hepatic iron overload induces hepatocellular carcinoma in transgenic mice expressing the hepatitis C virus polyprotein. Gastroenterology 2006, 130:2087–2098
9. Kim I, Rodriguez-Enriquez S, Lemasters JJ: Selective degradation of mitochondria by mitophagy. Arch Biochem Biophys 2007, 462:245–253
10. Elmore SP, Qian T, Grissom S, Lemasters JJ: The mitochondrial permeability transition initiates autophagy in rat hepatocytes. FASEB J 2001, 15:2286–2287
11. Matsuda N, Sato S, Shiba K, Okatsu K, Saisho K, Gautier CA, Sou YS, Saiki S, Kawajiri S, Sato F, Kimura M, Komatsu M, Hattori N, Tanaka K: PINK1 stabilized by mitochondrial depolarization recruits Parkin to damaged mitochondria and activates latent Parkin for mitophagy. J Cell Biol 2010, 189:211–221
12. Narendra DP, Jin SM, Tanaka A, Suen DF, Gautier CA, Shen J, Cookson MR, Youle RJ: PINK1 is selectively stabilized on impaired mitochondria to activate Parkin. PLoS Biol 2010, 8:e1000298
13. Geisler S, Holmström KM, Skujat D, Fiesel FC, Rothfuss OC, Kahle PJ, Springer W: PINK1/Parkin-mediated mitophagy is dependent on VDAC1 and p62/SQSTM1. Nat Cell Biol 2010, 12:119–131
14. Vives-Bauza C, Zhou C, Huang Y, Cui M, de Vries RL, Kim J, May J, Tocilescu MA, Liu W, Ko HS, Magrane J, Moore DJ, Dawson VL, Grailhe R, Dawson TM, Li C, Tieu K, Przedborski S: PINK1-dependent recruitment of Parkin to mitochondria in mitophagy. Proc Natl Acad Sci USA 2010, 107:378–383
15. Narendra D, Tanaka A, Suen DF, Youle RJ: Parkin is recruited selectively to impaired mitochondria and promotes their autophagy. J Cell Biol 2008, 183:795–803
16. Chan NC, Salazar AM, Pham AH, Sweredoski MJ, Kolawa NJ, Graham RL, Hess S, Chan DC: Broad activation of the ubiquitin-proteasome system by Parkin is critical for mitophagy. Hum Mol Genet 2011, 20:1726–1737
17. Gegg ME, Cooper JM, Chau KY, Rojo M, Schapira AH, Taanman JW: Mitofusin 1 and mitofusin 2 are ubiquitinated in a PINK1/parkin-dependent manner upon induction of mitophagy. Hum Mol Genet 2010, 19:4861–4870
18. Chen D, Gao F, Li B, Wang H, Xu Y, Zhu C, Wang G: Parkin mono-ubiquitinates Bcl-2 and regulates autophagy. J Biol Chem 2010, 285: 38214–38223
19. Narendra D, Kane LA, Hauser DN, Fearnley IM, Youle RJ: p62/SQSTM1 is required for Parkin-induced mitochondrial clustering but not mitophagy; VDAC1 is dispensable for both. Autophagy 2010, 6:1090–1106
20. Itakura E, Kishi-Itakura C, Koyama-Honda I, Mizushima N: Structures containing Atg9A and the ULK1 complex independently target depolarized mitochondria at initial stages of Parkin-mediated mitophagy. J Cell Sci 2012, 125:1488–1499
21. Okatsu K, Saisho K, Shimanuki M, Nakada K, Shitara H, Sou YS, Kimura M, Sato S, Hattori N, Komatsu M, Tanaka K, Matsuda N: p62/SQSTM1 cooperates with Parkin for perinuclear clustering of depolarized mitochondria. Genes Cells 2010, 15:887–900
22. Wakita T, Pietschmann T, Kato T, Date T, Miyamoto M, Zhao Z, Murthy K, Habermann A, Kräusslich HG, Mizokami M, Bartenschlager R, Liang TJ: Production of infectious hepatitis C virus in tissue culture from a cloned viral genome. Nat Med 2005, 11:791–796
23. Li K, Prow T, Lemon SM, Beard MR: Cellular response to conditional expression of hepatitis C virus core protein in Huh7 cultured human hepatoma cells. Hepatology 2002, 35:1237–1246
24. Lerat H, Honda M, Beard MR, Loesch K, Sun J, Yang Y, Okuda M, Gosert R, Xiao SY, Weinman SA, Lemon SM: Steatosis and liver cancer in transgenic mice expressing the structural and nonstructural proteins of hepatitis C virus. Gastroenterology 2002, 122:352–365
25. Tateno C, Yoshizane Y, Saito N, Kataoka M, Utoh R, Yamasaki C, Tachibana A, Soeno Y, Asahina K, Hino H, Asahara T, Yokoi T, Furukawa T, Yoshizato K: Near completely humanized liver in mice shows human-type metabolic responses to drugs. Am J Pathol 2004, 165:901–912
26. Kimura T, Imamura M, Hiraga N, Hatakeyama T, Miki D, Noguchi C, Mori N, Tsuge M, Takahashi S, Fujimoto Y, Iwao E, Ochi H, Abe H, Maekawa T, Arataki K, Tateno C, Yoshizato K, Wakita T, Okamoto T, Matsuura Y, Chayama K: Establishment of an infectious genotype 1b hepatitis C virus clone in human hepatocyte chimeric mice. J Gen Virol 2008, 89:2108–2113
27. Ando M, Korenaga M, Hino K, Ikeda M, Kato N, Nishina S, Hidaka I, Sakaida I: Mitochondrial electron transport inhibition in full genomic hepatitis C replicon cells is restored by reducing viral replication. Liver Int 2008, 28:1158–1166
28. Kim SJ, Syed GH, Siddiqui A: Hepatitis C virus induces the mitochondrial translocation of Parkin and subsequent mitophagy. PLoS Pathog 2013, 9:e1003285
29. Toida K, Kosaka K, Aika Y, Kosaka T: Chemically defined neuron groups and their subpopulations in the glomerular layer of the rat main olfactory bulb, IV: intraglomerular synapses of tyrosine hydroxylase-immunoreactive neurons. Neuroscience 2000, 101:11–17
30. Ikeda M, Sugiyama K, Mizutani T, Tanaka T, Tanaka K, Sekihara H, Shimotohno K, Kato N: Human hepatocyte clonal cell lines that support persistent replication of hepatitis C virus. Virus Res 1998, 56: 157–167
31. Zhang GJ, Liu HW, Yang L, Zhong YG, Zheng YZ: Influence of membrane physical state on the lysosomal proton permeability. J Membr Biol 2000, 175:53–62
32. Sharpe MA, Wrigglesworth JM, Loewen J, Nicholls P: Small pH gradients inhibit cytochrome c oxidase: implications for H+ entry to the binuclear center. Biochem Biophys Res Commun 1995, 216: 931–938
33. Hristova VA, Beasley SA, Rylett RJ, Shaw GS: Identification of a novel Zn2+-binding domain in the autosomal recessive juvenile Parkinson-related E3 ligase parkin. J Biol Chem 2009, 284:14978–14986
34. Sir D, Chen WL, Choi J, Wakita T, Yen TS, Ou JH: Induction of incomplete autophagic response by hepatitis C virus via the unfolded protein response. Hepatology 2008, 48:1054–1061
35. Dreux M, Gastaminza P, Wieland SF, Chisari FV: The autophagy machinery is required to initiate hepatitis C virus replication. Proc Natl Acad Sci U S A 2009, 106:14046–14051
36. Ke PY, Chen SS: Activation of the unfolded protein response and autophagy after hepatitis C virus infection suppresses innate antiviral immunity in vitro. J Clin Invest 2011, 121:37–56
37. Sir D, Kuo CF, Tian Y, Liu HM, Huang EJ, Jung JU, Machida K, Ou JH: Replication of hepatitis C virus RNA on autophagosomal membranes. J Biol Chem 2012, 287:18036–18043
38. Shrivastava S, Bhanja Chowdhury J, Steele R, Ray R, Ray RB: Hepatitis C virus upregulates Beclin1 for induction of autophagy and activates mTOR signaling. J Virol 2012, 86:8705–8712
39. Munafo DB, Colombo MI: A novel assay to study autophagy: regulation of autophagosome vacuole size by amino acid deprivation. J Cell Sci 2001, 114:3619–3629
40. Kurihara Y, Kanki T, Aoki Y, Hirota Y, Saigusa T, Uchiumi T, Kang D: Mitophagy plays an essential role in reducing mitochondrial production of reactive oxygen species and mutation of mitochondrial DNA by maintaining mitochondrial quantity and quality in yeast. J Biol Chem 2012, 287:3265–3272
41. Wang Y, Nartiss Y, Steipe B, McQibban GA, Kim PK: ROS-induced mitochondrial depolarization initiates PARK2/PARKIN-dependent mitochondrial degradation by autophagy. Autophagy 2012, 8:1462–1476
42. Nishikawa M, Nishiguchi S, Shiomi S, Tamori A, Koh N, Takeda T, Kubo S, Hirohashi K, Kinoshita H, Sato E, Inoue M: Somatic mutation of mitochondrial DNA in cancerous and noncancerous liver tissue in individuals with hepatocellular carcinoma. Cancer Res 2001, 61:1843–1845
43. Venditti P, Di Stefano L, Di Meo S: Mitochondrial metabolism of reactive oxygen species. Mitochondrion 2013, 13:71–82

JVI
Journals.ASM.org

Hallmarks of Hepatitis C Virus in Equine Hepacivirus

Tomohisa Tanaka,[a] Hirotake Kasai,[a] Atsuya Yamashita,[a] Kaori Okuyama-Dobashi,[a] Jun Yasumoto,[a] Shinya Maekawa,[b] Nobuyuki Enomoto,[b] Toru Okamoto,[c] Yoshiharu Matsuura,[c] Masami Morimatsu,[d] Noboru Manabe,[e] Kazuhiko Ochiai,[f] Kazuto Yamashita,[g] Kohji Moriishi[a]

Department of Microbiology, Faculty of Medicine, University of Yamanashi, Yamanashi, Japan[a]; First Department of Internal Medicine, Faculty of Medicine, University of Yamanashi, Yamanashi, Japan[b]; Department of Molecular Virology, Research Institute for Microbial Diseases, Osaka University, Osaka, Japan[c]; Laboratory of Laboratory Animal Science and Medicine, Department of Disease Control, Graduate School of Veterinary Medicine, Hokkaido University, Sapporo, Japan[d]; Animal Resource Science Center, Graduate School of Agricultural and Life Sciences, The University of Tokyo, Kasama, Japan[e]; Department of Basic Science, School of Veterinary Nursing and Technology, Faculty of Veterinary Science, Nippon Veterinary and Life Science University, Tokyo, Japan[f]; Department of Small Animal Clinical Sciences, School of Veterinary Medicine, Rakuno Gakuen University, Ebetsu, Hokkaido, Japan[g]

ABSTRACT

Equine hepacivirus (EHcV) has been identified as a closely related homologue of hepatitis C virus (HCV) in the United States, the United Kingdom, and Germany, but not in Asian countries. In this study, we genetically and serologically screened 31 serum samples obtained from Japanese-born domestic horses for EHcV infection and subsequently identified 11 PCR-positive and 7 seropositive serum samples. We determined the full sequence of the EHcV genome, including the 3′ untranslated region (UTR), which had previously not been completely revealed. The polyprotein of a Japanese EHcV strain showed approximately 95% homology to those of the reported strains. HCV-like *cis*-acting RNA elements, including the stem-loop structures of the 3′ UTR and kissing-loop interaction were deduced from regions around both UTRs of the EHcV genome. A comparison of the EHcV and HCV core proteins revealed that Ile^{190} and Phe^{191} of the EHcV core protein could be important for cleavage of the core protein by signal peptide peptidase (SPP) and were replaced with Ala and Leu, respectively, which inhibited intramembrane cleavage of the EHcV core protein. The loss-of-function mutant of SPP abrogated intramembrane cleavage of the EHcV core protein and bound EHcV core protein, suggesting that the EHcV core protein may be cleaved by SPP to become a mature form. The wild-type EHcV core protein, but not the SPP-resistant mutant, was localized on lipid droplets and partially on the lipid raft-like membrane in a manner similar to that of the HCV core protein. These results suggest that EHcV may conserve the genetic and biological properties of HCV.

IMPORTANCE

EHcV, which shows the highest amino acid or nucleotide homology to HCV among hepaciviruses, was previously reported to infect horses from Western, but not Asian, countries. We herein report EHcV infection in Japanese-born horses. In this study, HCV-like RNA secondary structures around both UTRs were predicted by determining the whole-genome sequence of EHcV. Our results also suggest that the EHcV core protein is cleaved by SPP to become a mature form and then is localized on lipid droplets and partially on lipid raft-like membranes in a manner similar to that of the HCV core protein. Hence, EHcV was identified as a closely related homologue of HCV based on its genetic structure as well as its biological properties. A clearer understanding of the epidemiology, genetic structure, and infection mechanism of EHcV will assist in elucidating the evolution of hepaciviruses as well as the development of surrogate models for the study of HCV.

The *Flaviviridae* family is composed of four genera: *Flavivirus*, *Pestivirus*, *Pegivirus*, and *Hepacivirus*. *Flaviviridae* family viruses are enveloped and contain a single-stranded, positive-sense RNA genome, which encodes a single large precursor polyprotein composed of approximately 2,800 to 3,000 amino acids. The genus *Hepacivirus* had included only two species, hepatitis C virus (HCV) and GB virus B (GBV-B), until 2010. GBV-B was isolated from serum samples obtained from laboratory tamarins by 11 passages of serum obtained from a human patient with idiopathic hepatitis (1). Although GBV-B experimentally infects tamarins and common marmosets, but not chimpanzees, *in vivo* (2, 3), the natural host of GBV-B has not yet been clarified. Several hepacivirus species were recently detected in dogs, horses, bats, and rodents and tentatively designated nonprimate hepaciviruses (NPHVs). Bat hepaciviruses have been isolated from some species of bats in Kenya (4), while rodent hepaciviruses have been isolated from several species of rodents in Germany, the Netherlands, South Africa, and Namibia (5, 6). GBV-B is phylogenetically more similar to rodent hepacivirus than to HCV (5). Several strains of equine hepacivirus (EHcV) have been isolated from domestic horses in the United States, the United Kingdom, and Germany (5, 7, 8). The canine hepacivirus was isolated from dogs in the United States (9) but has not yet been genetically or serologically detected in any dogs other than those from the first report (5, 7, 8). The polypeptides of canine hepacivirus show approximately 95% amino acid homology to those of the EHcV strains, suggesting that canine hepacivirus may belong to the same species as EHcV and

Received 8 August 2014 Accepted 2 September 2014
Published ahead of print 10 September 2014
Editor: T. S. Dermody
Address correspondence to Kohji Moriishi, kmoriishi@yamanashi.ac.jp.

doi:10.1128/JVI.02280-14

that infections may be rare in dogs (5, 7, 8, 10). Recent phylogenetic analyses identified EHcV as the most closely related viral homologue of HCV among the reported NPHV strains; however, epidemiological and virological information on EHcV is limited. The open reading frames of EHcV strains show approximately 95% homology to one another, suggesting that previously reported EHcV strains may be classified into one species. Several genome sequences of rodent hepacivirus have already been completely determined (5). The 3′ untranslated region (UTR) of HCV was found to include three stem-loop (SL) structures, while variable stem-loop structures were found in that of rodent hepacivirus and GBV-B (5). However, the nucleotide sequence of the EHcV 3′ UTR has not yet been determined completely because the adenine-rich [(A)-rich] sequence downstream of the stop codon in the EHcV genome interrupts an ordinary 3′-rapid amplification of cDNA ends (RACE) reaction (8). The RNA secondary structure of the hepacivirus 3′ UTR may indicate species specificity (5).

On the basis of amino acid similarities among the polyproteins of NPHVs and HCV, the N-terminal one-fourth of the NPHV polyprotein has been predicted to be cleaved by signal peptidase into mature structural proteins and a viroporin (core, E1, E2, and p7), while the C-terminal three-fourths has been predicted to be cleaved by viral proteases into maturated nonstructural proteins (NS2, NS3, NS4A, NS4B, NS5A, and NS5B) (6). Core, E1, and E2 have been predicted to form viral particles with host lipids, although it remains unclear whether p7 is incorporated into a viral particle. Signal peptide peptidase (SPP) was shown to further cleave the C-terminal transmembrane region of HCV and GBV-B core protein after signal peptidase-dependent cleavage (11, 12). However, whether SPP cleaves the C-terminal transmembrane region of the NPHV core protein remains unknown.

The mature core proteins of HCV and GBV-B are localized mainly on lipid droplets (LDs) (13, 14). The core proteins of dengue virus are also localized on LDs but are not cleaved by SPP (15), suggesting that localization of the core protein on LDs may be one of the common characteristics of the *Flaviviridae* family. The HCV core protein is known to be partially localized in the detergent-resistant membrane (DRM), which originates from lipid raft-like membranes (16, 17). The DRM is composed of cholesterol and sphingolipids, which are included in the replication compartment known as the membranous web (18, 19). Therefore, LDs and DRM are considered to be the intracellular compartments for the replication and viral assembly of HCV, but it is currently unknown whether NPHV core proteins are localized on LDs and DRM.

Epidemiological information on EHcV is still limited. The results of the present study demonstrated that Japanese-born domestic horses were infected with EHcV, which showed high homology to the reported strains on the basis of its nucleotide and amino acid sequences. We predicted the RNA secondary structures around the 5′ and 3′ UTRs of the EHcV genome and analyzed the biological properties of the EHcV core protein in relation to the HCV core protein.

MATERIALS AND METHODS

Samples. Serum samples 1 to 13 were collected from Japanese-born domestic horses raised on one farm, farm A, located in Hokkaido, Japan, while groups of serum samples numbered 14 to 18 and 19 to 31 were from horses on farms B and C, respectively, located in Tokyo, Japan (Fig. 1). The distance between Hokkaido and Tokyo is about 1,000 km. All sample collections conformed to guidelines for the care and use of laboratory animals (Yamanashi University) and were approved by the Institutional Committee of Laboratory Animal Experimentation (Yamanashi University). All samples were divided into small aliquots and stored at −80°C until nucleic acid extraction.

RT-PCR. Total RNAs were prepared from horse sera using a Qiagen viral RNA extraction kit (Qiagen, Valencia, CA). RNAs were converted to cDNA using a PrimeScript reverse transcription-PCR (RT-PCR) kit (TaKaRa, Shiga, Japan) with random primers. The viral gene was amplified by PCR using PuReTaq Ready-To-Go PCR beads (GE Healthcare, Piscataway, NJ) with three pairs of primers: NPHV-F1 (5′-TGTCACCT ACTATCGGGG-3′) and NPHV-R1 (5′-TCAAGCCTATACAGCAAAG G-3′), NPHV-F2 (5′-ATCATTTGTGATGAGTGCC-3′) and NPHV-R2 (5′-CATAAGGGCGTCCGTGGC-3′), and NPHV-F3 (5′-GTGGTCGCC ACGGATGCC-3′) and NPHV-R3 (5′-ACCCTATGAAGACGCTCTCC-3′). PCR was carried out as follows: one cycle at 92°C for 5 min; 35 repeats of one cycle at 94°C for 0.5 min, 58°C for 0.5 min, and 72°C for 0.5 min, in that order; and one cycle at 72°C for 1 min followed by holding at 4°C. The PCR products were electrophoresed on 1.5% agarose gels, stained with ethidium bromide, and visualized using the BioDoc-It imaging system (UVP, Upland, CA).

Determination of the EHcV genomic sequence. The viral genome of EHcV was segmentally amplified by PCR using the primers listed in Table 1. The PCR products were cloned into T vectors prepared from pBluescript II SK(−) (20). The DNA sequences of the PCR products were determined using an ABI Prism BigDye Terminator version 1.1 cycle sequencing kit and an ABI Prism 310 genetic analyzer (Life Technologies, Tokyo, Japan). More than three colonies were picked up among the transformants of *Escherichia coli* with regard to the accuracy of the sequence. The nucleotide sequences of the PCR products were determined in forward and reverse directions. The junction of two adjacent PCR products was confirmed by PCR using primers that overlapped two close regions. The 5′-terminal sequence upstream of the open reading frame was determined with a 5′-RACE core set (TaKaRa) using the 5′ phospholyrated RT primer for the NPHV 5′ UTR (5′-CATCCTATCAGACCG-3′). The 3′-terminal region downstream of the (A)-rich region was determined by the 3′-RACE method (21, 22), modified as follows: Total RNAs were prepared from horse serum using TRIzol LS reagent (Invitrogen, Carlsbad, CA) with 40 μg of glycogen (Nacalai Tesque, Kyoto, Japan). The poly(U) tail was added to the 3′ end of the RNA preparation using *Escherichia coli* poly(U) polymerase (New England BioLabs, Ipswich, MA) and was incubated for 45 min at 37°C. The resulting preparation was reverse transcribed by the SuperScript First-Strand Synthesis system (Life Technologies) using an oligo(dA) adapter primer (5′-TTGCGAGCACAGAATTAATACG ACTCACAAAAAAAAAAAAVN-3′). The sequence of each region was determined by sequencing more than 3 clones. The primers for PCR amplification and the RACE methods are listed in Table 1. The whole sequence of the EHcV strain isolated from serum sample 3 (GenBank accession number AB863589) was determined by the method described above. The EHcV strain was designated JPN3/JAPAN/2013 in this study. The partial NS5B-coding regions and 3′ UTRs were amplified from serum samples 5 and 1. The nucleotide sequences of samples 5 and 1 (GenBank accession numbers AB921150 and AB921151, respectively) were determined by the method described above. The neighbor-joining trees of the nucleotide sequences from the NPHV, HCV, and GBV-B strains were predicted by the method of Saitou et al (23). Trees were constructed by the maximum composite likelihood method calculated by using the program MEGA5 (24) (see Fig. 3). The secondary protein structures were predicted by the method of Garnier et al. (25) (see Fig. 6). Hydrophobicity plots of the EHcV and HCV core proteins were prepared by the method of Kyte and Doolittle (26) and drawn using the software Genetyx (Nihon Genetyx, Tokyo, Japan) (see Fig. 5).

Quantification of viral genomic RNAs in horse sera. Total RNA was prepared from equine serum using a Qiagen viral RNA extraction kit and was then reverse transcribed into cDNA by using a PrimeScript RT-PCR

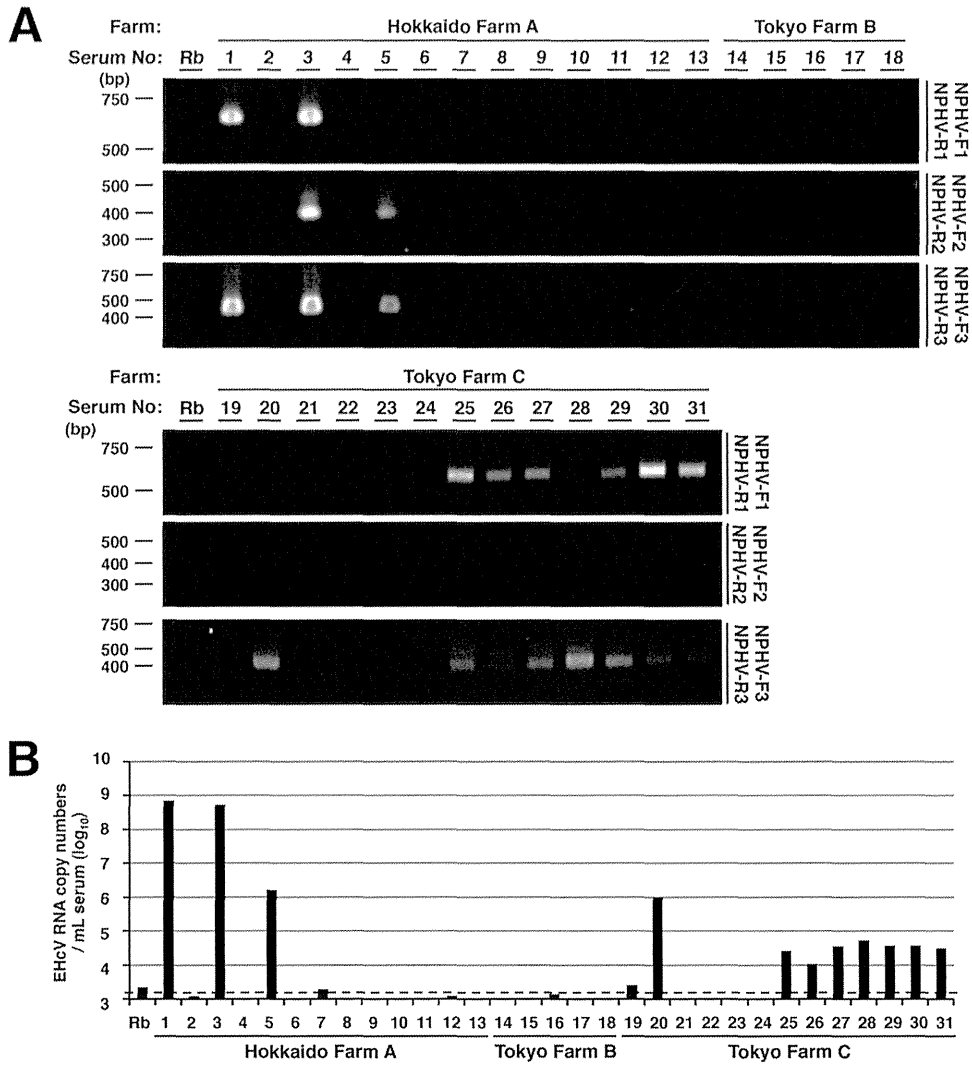

FIG 1 Detection and genetic analyses of NPHV genomic RNA in sera of Japanese domestic horses. (A) Total RNAs extracted from 31 equine sera and normal rabbit serum (Rb) as a negative control were subjected to RT-PCR analysis. Hokkaido Farm A, Tokyo Farm B, and Tokyo Farm C indicate the farms where the individual horses were reared. Three sets of primers, NPHV-F1 and NPHV-R1, NPHV-F2 and NPHV-R2, and NPHV-F3 and NPHV-R3, were used to amplify NPHV-specific gene regions. The PCR products were electrophoresed and stained with ethidium bromide. (B) Total RNAs were isolated from sera, reverse-transcribed, and estimated as a copy number per ml. Normal rabbit serum was used as a negative control. The dashed line indicates the cutoff level.

kit with random primers. The amount of targeted viral RNA was estimated using SYBR GreenER qPCR SuperMix (Life Technologies) and the ABI StepOnePlus real-time PCR system (Life Technologies). The region encoding NS3 was targeted with the primer pair NPHV-F3 (5′-GTGGTC GCCACGGATGCC-3′) and NPHV-R3 (5′-ACCCTATGAAGACGCTC TCC-3′). Total RNAs extracted from conventional rabbit serum were used as a negative control to determine the analytical threshold line. The *in vitro*-transcribed RNA of EHcV was utilized for the standard curve.

Prediction of RNA secondary structures. The 5′-UTR sequences of EHcV strains were aligned with the MUSCLE program and subjected to a manual search for covariant nucleotide substitutions. The RNA folding structure upstream of domain III in the 5′ UTR was predicted using the Mfold web server (27) with conventional phylogenetic conservation analysis due to the lack of sufficient homology to the 5′ UTR sequences of HCV strains. The NS5B-coding regions and 3′ UTRs of EHcV strains were aligned with the program MUSCLE. Conserved secondary structures were predicted as described above. The secondary structures of the 3′ UTR in EHcV were predicted by the Mfold web server without confirming phylogenetic data because of the absence of additional available sequences of the EHcV 3′ UTR and the lack of sufficient homology to the HCV X-tail sequences.

Plasmids. The PCR product encoding the EHcV core protein was amplified from serum sample 3 and was then cloned into the BamHI and XhoI sites of pcDNA3.1-Flag/HA, which encodes the FLAG and hemagglutinin (HA) epitope tags, as reported previously (28). Ala^{204} was replaced with Lys to prevent signal peptidase-dependent cleavage. The translated EHcV core protein was added to the FLAG and HA epitope tags at the N and C termini (EHcVc), respectively. A point mutation was generated using a KOD mutagenesis kit (Toyobo, Osaka, Japan). The PCR products encoding EHcVc or the mutant in which Ile^{190} and Phe^{191} were replaced with Ala and Leu (EHcVc-mt), respectively, were introduced into the AflII and EcoRV sites of pCAGGS using an In-Fusion HD cloning kit (TaKaRa). The introduced fragments of all plasmids were confirmed by sequencing using an ABI Prism 310 genetic analyzer (Applied Biosystems). The plasmid encoding the N-terminally FLAG-tagged and C-terminally HA-tagged HCV core protein (HCVc) and the mutant in which

TABLE 1 List of PCR primers used in this study

Primer	Nucleotide position	Genome location	F or R[a]	Sequence (5′→3′)
Primer for cloning of the NPHV genome	92–111	5′ UTR	F	ATGTGTCACTCCCCCTATGG
	367–386	5′ UTR	R	CTATGGTCTACGAGACCGGC
	268–285	5′ UTR	F	AGCCGAAATTTGGGCGTG
	1207–1224	E1	R	AAACAGAAGCCATAGCGG
	1116–1132	E1	F	AGTGCTTGTTGGGTGCC
	1697–1713	E2	R	GTCCTTTGCACTTCGGG
	1605–1623	E2	F	ACTGTTAAGCAGATGTGGG
	2103–2121	E2	R	CACAGAGTTGGTAAGTAGC
	2007–2023	E2	F	AAGCAGTGTGGTGCTCC
	2526–2545	E2	R	AAACAGAACCAGAGAATTGC
	2375–2392	E2	F	CCCTGCCTTCACTACTGG
	2898–2913	NS2	R	CGAGATAGCGCCAAGC
	2847–2867	NS2	F	TTTATGCTAGTAAAGTGGTGG
	3396–3415	NS2	R	GGTGATAAAAGTCTCCATCC
	3318–3334	NS2	F	ATCCTCCATGGCTTGCC
	3819–3835	NS3	R	GGGCCACCTGAACTACC
	3732–3750	NS3	F	ACCAGGACGGGTCAGGTCG
	4254–4270	NS3	R	ATAATGTCATAAGCACC
	4177–4195	NS3	F	CTAGTTGCAAGACAACGGG
	4682–4700	NS3	R	AGTGTTGCAGTCAGTGACG
	4574–4591	NS3	F	TGTCACCTACTATCGGGG
	5199–5218	NS3	R	TCAAGCCTATACAGCAAAGG
	4574–4591	NS3	F	TGTCACCTACTATCGGGG
	5199–5218	NS3	R	TCAAGCCTATACAGCAAAGG
	5134–5152	NS3	F	CTCCCAGCAAAGATGAACG
	5997–6014	NS4B	R	AGCACCCACACCAACAGC
	5919–5934	NS4B	F	AAGATCTTGAGTGGTG
	6651–6632	NS5A	R	GCCGATAACTCTGACAGC
	6547–6564	NS5A	F	ACACCTGGAAAACAGCCG
	7293–7310	NS5A	R	AGATTCCGTGGCCGAAGG
	7235–7252	NS5A	F	AGCTCTCGTTTCCGGGTG
	7573–7590	NS5B	R	TAGCTGACGCTGTTGTGG
	7511–7527	NS5B	F	ACGCCACCCTATAGGCC
	8027–8046	NS5B	R	GTTGACGGGGAGTGTATTGG
	7926–7943	NS5B	F	ATCGTTTACCCCGATTTG
	8528–8545	NS5B	R	CAAGATGTTATCTGCTCC
	8457–8474	NS5B	F	CGTGACTTCACTAATGCC
	9069–9086	NS5B	R	GTCAATCGAGTTTACGCC
Primer for 5′ RACE	235–252	5′ UTR	F	AATCGCGGCTTGAACGTC
	213–230	5′ UTR	R	TGTACTCACGGATTCACG
Primer for 3′ RACE	8979–8999	NS5B	F	CTTAAAGTACGTGGTGGTCGC
Adapter primer			R	GCGAGCACAGAATTAATACGAC

[a] F, forward; R, reverse.

Ile[176] and Phe[177] were replaced with Ala and Leu (HCVc-mt), respectively, were described previously (28). The gene encoding human signal peptide peptidase (SPP) or its mutant was introduced into pcDNA3.1-myc/His C (Invitrogen) instead of the plasmids described previously (28). The resulting plasmids encoded C-terminally myc-$His_{\times 6}$-tagged wild-type SPP (SPP-wt) or the mutant protein in which Asp[219] was replaced with Ala (SPP-D219A).

Cell culture and transfection. The human embryonic kidney cell line 293FT and the human hepatoma cell line Huh7OK1 (29) were maintained in Dulbecco's modified Eagle's minimal essential medium (DMEM) supplemented with 100 U/ml penicillin, 100 μg/ml streptomycin, nonessential amino acids (Sigma, St. Louis, MO), sodium pyruvate (Sigma), and 10% fetal bovine serum (FBS) and were then cultured at 37°C under the conditions of a humidified atmosphere and 5% CO_2. Plasmids were transfected into cell lines using XtremeGene 8 (Roche) according to the manufacturer's protocol.

Western blot analysis. 293FT cells were cultured in 6-well plates and transfected with the appropriate plasmids. The transfected cells were harvested at 18 h posttransfection, washed with cold phosphate-buffered saline (PBS), and suspended in 50 μl of the lysis buffer consisting of 20 mM Tris-HCl (pH 7.5), 135 mM NaCl, 10% glycerol, 1% Triton X-100, and protease inhibitor cocktail (Merck Bioscience, Calbiochem, San Diego, CA). The lysates were centrifuged at 19,000 × *g* for 5 min at 4°C. The supernatants were mixed with 16 μl of 4× SDS sample buffer and then boiled at 60°C for 20 min. The resulting mixtures were subjected to SDS-PAGE. The proteins in a gel were transferred to polyvinylidene difluoride (PVDF) membranes and incubated with mouse anti-FLAG antibodies (Sigma), mouse anti-HA antibodies (Covance, Princeton, NJ), mouse

anti-c-*myc* antibodies (BD Pharmingen, San Diego, CA), or mouse anti-beta-actin antibodies (Santa Cruz Biotechnology, Santa Cruz, CA) and were then incubated with the appropriate horseradish peroxidase (HRP)-conjugated secondary antibodies. Immunocomplexes were visualized with SuperSignal West Femto substrate (Thermo Scientific, Rockford, IL) and detected using an LAS-4000 Mini image analyzer (GE Healthcare, Buckinghamshire, United Kingdom).

Detection of antibodies against EHcV. To detect anti-EHcV antibodies in horse sera, we subjected lysates prepared from 293FT cells expressing EHcVc, which is an N-terminally FLAG-tagged and C-terminally HA-tagged EHcV core protein (a positive reference), or cells transfected with an empty plasmid (a negative reference) to Western blotting, as described above. The resulting PVDF membranes were incubated with Blocking One solution (Nacalai Tesque) for blocking at room temperature for 30 min and then incubated with 1,000-fold-diluted horse serum in 10-fold-diluted Blocking One. Mouse anti-FLAG or rabbit anti-EHcV core antibody was used as a positive serum control. The resulting membrane was incubated with an HRP-conjugated antibody to mouse, rabbit, or horse IgG (Abcam, Cambridge, UK) at room temperature for 1 h. Protein bands with a molecular mass of 28 kDa were detected in the positive reference, but not in the negative reference, using positive serum or an antibody to the FLAG epitope tag or EHcV core protein. The rabbit polyclonal antibody against the EHcV core protein was generated by immunization using peptides of the residues from 2 to 15, GNKSKNQKPQPQRG (Scrum Inc., Tokyo, Japan).

Pulldown assay for SPP binding. Human embryonic kidney 293FT cells expressing EHcVc or HCVc with or without SPP-D219A were harvested at 18 h posttransfection, washed with cold PBS, suspended in 100 μl of the lysis buffer, and centrifuged at 14,000 ×g for 5 min at 4°C. Twenty microliters of the lysate was mixed with 20 μl of 2× SDS sample buffer. The remaining lysate was adjusted to 250 μl with the lysis buffer and incubated for 2 h at 4°C after the addition of 20 μl of His-Select nickel affinity gel (Sigma) equilibrated 50% (vol/vol) with lysis buffer. The nickel beads that included SPP-wt or SPP-D219K were washed five times with 500 μl of lysis buffer by centrifugation at 5, 000 × *g* for 1 min at 4°C and then suspended in 40 μl of 1× SDS sample buffer. After being boiled at 60°C for 20 min, the supernatant was subjected to Western blotting to detect the coprecipitated core proteins.

Immunofluorescence microscopy. Huh7OK1 cells were incubated with fresh DMEM containing Bodipy 558/568 (2 μg/ml; Molecular Probes) for 1 h at 37°C to visualize lipid droplets (LDs). The cells were washed once with prewarmed DMEM and incubated for 30 min at 37°C. The treated cells were then fixed in 4% paraformaldehyde for 30 min at room temperature. After two washes with PBS, the cells were permeabilized with permeabilization buffer containing 0.1% saponin (eBioscience, San Diego, CA) for 30 min at 37°C and blocked with PBS containing 2% FBS (blocking buffer) for 30 min at room temperature. The cells were incubated with an appropriate antibody, as indicated in the figure legends. The cells were washed three times with PBS. The mounted cells were observed with a FluoView FV1000 laser scanning confocal microscope (Olympus, Tokyo, Japan). Nuclei were stained with 4′,6′-diamidino-2-phenylindole (DAPI).

Flotation assay. A flotation assay was carried out according to the method described previously (17). Briefly, 293FT cells expressing EHcVc or EHcVc-mt were cultured on a 10-cm dish. The transfected cells were washed once with cold PBS at 18 h posttransfection and harvested using a cell scraper. The cells were suspended in 1.2 ml of 25 mM Tris-HCl (pH 7.5) containing 150 mM NaCl, 5 mM EDTA, and protease inhibitor cocktail (Merck, Calbiochem) (TNE buffer) and were then homogenized by 10 passes through a 26-gauge needle. Each 0.6-ml aliquot of the homogenates was incubated for 30 min on ice with or without 1% Triton X-100 and was then mixed with 0.4 ml of OptiPrep (Axis-Shield, Oslo, Norway). An appropriate concentration of OptiPrep was adjusted with TNE buffer. This mixture was overlaid with 1.2 ml of 30% OptiPrep, 1.2 ml of 25% OptiPrep, and 0.8 ml of 5% OptiPrep, in that order, and was centrifuged at 42,000 rpm for 5 h at 4°C in an SW50.1 rotor (Beckman Coulter, Fullerton, CA). Each fraction, with a volume of 0.4 ml, was collected from the top of the centrifugation tube and was then precipitated by mixing with 4 volumes of cold acetone at −30°C. The resulting pellet was resolved in 50 μl of 1× sample buffer and then subjected to Western blot analysis using a mouse anti-FLAG antibody (Sigma), a rabbit anti-calreticulin antibody (Sigma), and a rabbit anti-caveolin-1 antibody (Sigma). The fractions containing calreticulin in the absence and presence of Triton X-100 were defined as the membrane and detergent-soluble membrane fractions, respectively. In the presence of the detergent, fractions 3 to 5, which contained caveolin-1 but only small amounts of calreticulin, were defined as the detergent-resistant membrane fractions.

Nucleotide sequence accession numbers. The whole sequence of the EHcV strain isolated from serum sample 3 was deposited in GenBank under accession number AB863589. The nucleotide sequences of the partial NS5B-coding regions and 3′ UTRs from samples 5 and 1 were registered as AB921150 and AB921151, respectively.

RESULTS

Detection of the EHcV genome and antibody to EHcV in sera of Japanese-born horses. To clarify whether NPHVs were distributed in Japan, we collected 31 horse serum samples and examined them in order to detect the EHcV genome and antibody to the core protein. We prepared total RNAs from horse sera and screened them using RT-PCR analyses with three sets of PCR primers (NPHV-F1/NPHV-R1, NPHV-F2/NPHV-R2, and NPHV-F3/NPHV-R3) that targeted the NS3-coding region that is relatively conserved among NPHVs. Total RNA prepared from conventional rabbit serum was used as a negative control. PCR products with the expected sizes were found in horse serum samples 1, 3, 25, 26, 27, and 29 to 31 using NPHV-F1/NPHV-R1, in horse serum samples 3 and 5 using NPHV-F2/R2, and in horse serum samples 1, 3, 5, 20, and 25 to 31 using NPHV-F3/R3 (Fig. 1A). The EHcV genome was detected in 11 of 31 (35%) serum samples by RT-PCR (Fig. 1A and B). Copy numbers of the EHcV genome in horse sera varied from 10^4 to 10^9 copies per ml of sera (Fig. 1B). Although a PCR product was slightly amplified from serum sample 19 by PCR using the primer pair NPHV-F1/R1, the copy number of the virus genome in serum sample 19 was estimated to be low, at a level similar to that of the negative control. Thus, we could not determine whether serum sample 19 included a viral genome. We then immunologically surveyed horse sera by Western blotting. Western blotting analyses using horse sera to detect antibodies to the EHcV core protein (Fig. 2) showed that the sera of samples 1, 2, 3, 5, 14, 20, and 25 were immunoreactive to the EHcV core protein (7 positive serum samples of a total of 31 samples; 22.6%). The sera of samples 1, 3, 5, and 20 were PCR positive and seropositive. Serum samples 2 and 14 were PCR negative and seropositive, whereas samples 26 to 31 were PCR positive and seronegative. These results suggest that EHcV has infected Japanese-born domestic horses.

Genetic analysis of EHcV. PCR products corresponding to the 5′ UTR and the open reading frame were segmentally amplified from serum sample 3 by 5′ RACE and RT-PCR, respectively. In the present study, we successfully determined the 3′-terminal sequence downstream of a stop codon using the 3′-RACE method with poly(U) polymerase. We determined the nucleotide sequence of the putative full genome, which was designated JPN3/JAPAN/2013 (GenBank accession number AB863589). The full-length genome of strain JPN3/JAPAN/2013 is composed of 9,355 nucleotides, consisting of the 5′ UTR with a nucleotide length of 389, the 3′ UTR with a nucleotide length of 134, and an open

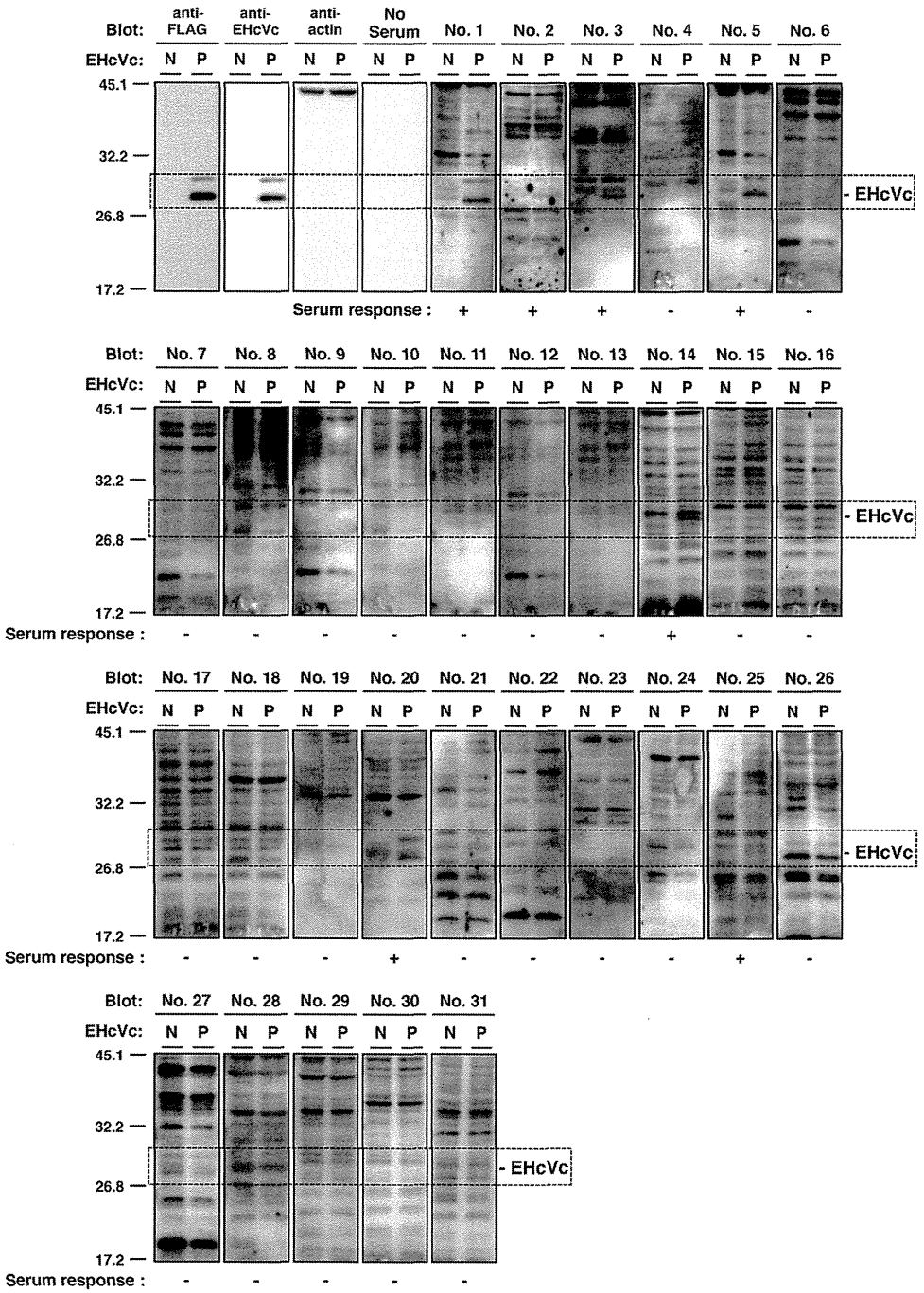

FIG 2 Serological screening of Japanese-born domestic horses. Lysates of 293FT cells transfected with an empty plasmid (a negative reference, N) or the plasmid encoding EHcVc (a positive reference, P) were subjected to Western blotting using serum from each horse. The serum response "+" indicates that the protein band with the same molecular size as the EHcV core protein was specifically detected in the "P" lane, but not in the "N" lane, while the serum response "−" indicates that the protein band with the same molecular size as the EHcV core protein was detected in neither the "P" lane nor the "N" lane. Both antibodies to the FLAG tag and to the EHcV core protein were used as serum positive controls, while protein amounts were standardized with blotting using the antibody to beta-actin. "No serum" indicates the membrane was incubated without primary antibodies but with HRP-conjugated anti-horse IgG antibodies as a background of the secondary antibody.

reading frame with a nucleotide length of 8,832. The open reading frame encodes 2,943 amino acids. Table 2 summarizes the amino acid homology of the JPN3/JAPAN/2013 polyprotein with the polyproteins of the other EHcV strains. The polyprotein of JPN3/JAPAN/2013 shared more than 94% homology with the other EHcV polyproteins and exhibited the highest homology, 97.8%, with NPHV-H10-094 (GenBank accession number JQ434007), which was isolated from a horse in the United States (8). The NS3- and NS5B-coding regions of the EHcV strains were phylogenetically analyzed by the neighbor-joining method. The phylogenetic

TABLE 2 Amino acid sequence homologies of the polyproteins

	Non-primate hepaciviruses					
	H10-094 (JQ434007)	B10-022 (JQ434004)	NZP1 (JQ434001)	AAK-2011 (JF44991)	H3-011 (JQ434008)	A6-066 (JQ434003)
JPN3/JAPAN/2013 (AB863589)	97.8[a]	96.7	95.7	95.7	95.6	95.3

	Non-primate hepaciviruses		HCV			
	G1-073 (JQ434002)	F8-068 (JQ434005)	HCV1a (NC004102)	HCV1b (AB779562)	JFH1 (AB047639)	GBV-B (NC001655)
JPN3/JAPAN/2013 (AB863589)	94.9	94.1	46.5	45.6	44.5	28.9

	Non-primate hepaciviruses		
	JPN3/JAPAN/2013 (AB863589)	AAK-2011 (JF44991)	GBV-B (NC001655)
HCV1a (NC004102)	46.1	46.0	33.3

[a], percent identity.

trees of the NS3 (Fig. 3A) and NS5B regions (Fig. 3B) showed that JPN3/JAPAN/2013 was included in the clade comprising the U.S. strains NPHV-H10-094 (GenBank accession number JQ434007) and B10-022 (GenBank accession number JQ434004).

Putative RNA secondary structures around the UTRs of EHcV. The 5′-terminal region of JPN3/JAPAN/2013 was compared with those of the EHcV genomes (Fig. 4A). The HCV internal ribosome entry site (IRES)-like structure was embedded in the 5′ UTRs of NPHVs (5, 6). The 5′-UTR region was well conserved among the EHcV strains and showed a mean diversity of approximately 4% among the EHcV strains (Fig. 4A). The 3′-terminal sequence downstream of the (A)-rich region in the EHcV genome had not been reported because the (A)-rich region downstream of the stop codon of EHcV interrupted the reaction in the ordinary 3′-RACE method (5, 6). In the present study, we determined the nucleotide sequences downstream of the (A)-rich region from serum sample 3 (JPN3/JAPAN/2013; GenBank accession number AB863589), sample 5 (JPN5/JAPAN/2015; GenBank accession number AB921150), and sample 1 (JPN1/JAPAN/2015; GenBank accession number AB921151) by the modified 3′-RACE method using poly(U) polymerase, although the region in serum sample 1 was incompletely amplified (Fig. 4B). The regions downstream of the (A)-rich region were conserved between serum samples 3 and 5, whereas the (A)-rich regions varied among the three strains (Fig. 4B).

The secondary structure of 5′ UTR in strain JPN3/JAPAN/2013 was predicted according to the method described previously (8) (Fig. 4C). The stem-loops in the 5′ UTR were designated according to the stem-loops of the HCV 5′-UTR structures (30). Stem-loops (SLs) I, II, IIIa to IIIf, and the pseudoknot interaction were predicted within the 5′ UTR of strain JPN3/JAPAN/2013. These structures were the same as that of the strain reported previously (9), although several nucleotide insertions and deletions were more predominant in the apical loop of subdomain IIIb than in the other strains reported previously (Fig. 4A and C). Two seed sites of the microRNA miR-122 (Fig. 4A and C) were found in the 5′ UTR of strain JPN3/JAPAN/2013 at nucleotide residues 81 to 89 (UCCACAUUA) and 98 to 103 (CACUCC), which also corresponded to the predicted miR-122 seed sites in the 5′ UTRs of the other EHcV strains (9).

The HCV 3′ UTR, which is generally 200 to 300 nucleotides in length, consists of a short variable region, the poly(U/UC) stretch sequence, and the 3′-X-tail region, in that order (31–33). Although the EHcV 3′ UTR, which is composed of 138 nucleotides, is shorter than the HCV 3′ UTR, the 3′ UTR of EHcV consists of the (A)-rich sequence and 3′-X-tail region, in that order. The (A)-rich sequence of EHcV may vary in length (Fig. 4B). We subsequently predicted the secondary structure of the EHcV 3′ UTR. Although the EHcV 3′ UTR, which is composed of 138 nucleotides, is shorter than the HCV 3′ UTR, the 3′ UTR includes three predicted SL structures (Fig. 4C). Based on the SL structures in the HCV 3′ X-tail, these SL structures in the EHcV 3′ UTR were designated 3′SL I, 3′SL II, and 3′SL III, in that order from the 3′ terminus (Fig. 4C). Interestingly, the (A)-rich sequence was partially incorporated into the 3′SL III, although the poly(U/UC) stretch sequence in the HCV 3′ UTR is separated from any 3′SL structures (31–33). Furthermore, the two SL structures in the 3′ side of the EHcV NS5B-coding region were predicted to correspond to 5BSL3.2 and 5BSL3.3 in the NS5B-coding region of HCV. HCV 5BSL3.2 was previously shown to interact with 3′SL II to form the kissing-loop interaction, which is required for HCV replication (33). The secondary structure prediction shown in Fig. 4C suggests that the kissing-loop interaction may be conserved between 5BSL3.2 and the 3′SL II of the EHcV genome through their complementary sequences. The long-range RNA-RNA interaction between the apical loop of subdomain IIId in HCV IRES and the bulge of 5BSL3.2 supports IRES-dependent translation and viral RNA replication (34–36). In the case of the EHcV genome, the complement sequences were detected in the apical loops of subdomain and the 5BSL3.2-like subdomain (Fig. 4C), suggesting that the long-range RNA-RNA interaction may reside in the EHcV genome. These results indicated that HCV-like RNA secondary structures may be conserved around both UTRs of the EHcV genome.

Cleavage of the EHcV core protein by SPP. The C-terminal transmembrane region of the HCV core protein was previously shown to be cleaved by SPP following the cleavage of the core-E1 junction by signal peptidase (11, 28, 37). The core protein is known to be released from the precursor polyprotein embedded in the endoplasmic reticulum (ER) membrane, and it then moves

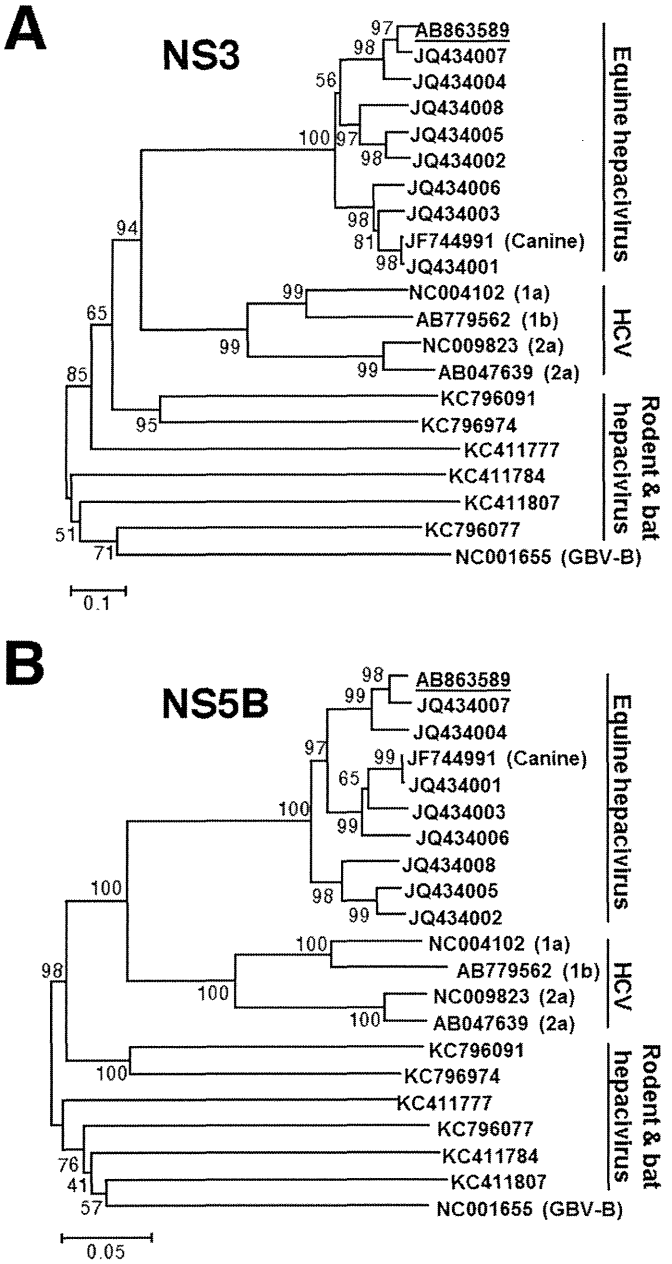

FIG 3 Phylogenetic analysis of the EHcV gene. Neighbor-joining trees of the nucleotide sequences from the NS3 (A) and NS5B (B) regions of the NPHV, HCV, and GBV-B strains are shown (23). Trees were constructed by the maximum composite likelihood method calculated using the program MEGA5 (24). The percentage of replicate trees in which the associated taxa were clustered together in the bootstrap test (1,000 replicates) is indicated next to the branches. Analyses were carried out using 10 strains of EhcV, JPN3/JAPAN/2013, A6-066 (GenBank accession no. JQ434003), B10-022 (GenBank accession no. JQ434004), F8-068 (GenBank accession no. JQ434005), G1-073 (GenBank accession no. JQ434002), G5-077 (GenBank accession no. JQ434006), H3-011 (GenBank accession no. JQ434008), H10-094 (GenBank accession no. JQ434007), NZP1 (GenBank accession no. JQ434001), and AAK-2011 (canine hepacivirus; GenBank accession no. JF744991); 4 strains of HCV, H77 (genotype 1a; GenBank accession no. NC004102), LyHCV (genotype 1b; GenBank accession no. AB779562), HC-J6CH (genotype 2a; GenBank accession no. NC009823), and JFH1 (genotype 2a; GenBank accession no. AB047639); 3 strains of bat hepacivirus, PDB-112 (GenBank accession no. KC796077), PDB-445 (GenBank accession no. KC796091), and PDB-829 (GenBank accession no. KC796074); 3 strains of rodent hepacivirus, RMU10-3382 (GenBank accession no. KC411777), NLR-AP-70 (GenBank accession no. KC411784), and SAR-46 (GenBank accession no. KC411807); and another primate hepacivirus, GBV-B (GenBank accession no. NC001655). The Japanese strain JPN3/JAPAN/2013 (GenBank accession no. AB863589) is underlined.

mainly to lipid droplets (LDs) (13, 14). Although SPP-dependent cleavage and LD translocation of the capsid protein are features common to HCV and GBV-B (13), it currently remains unknown whether the EHcV core protein shows these properties. The EHcV core protein shared 49.5% amino acid homology with the HCV core protein (genotype 1b) (Fig. 5A) and exhibited a hydrophobic/hydrophilic pattern similar to that of the HCV core protein (Fig. 5B). The EHcV core protein was predicted to be composed of domains 1, 2, and 3 relative to the HCV core protein. The transmembrane region of the EHcV core protein was predicted to span from Asn^{177} to Val^{199} by TMHMM2.0 (http://www.cbs.dtu.dk/services/TMHMM/). The transmembrane region of the EHcV core protein was 65% identical to that of the HCV core proteins (Fig. 5A). The C-terminal residue of the mature HCV core protein was found to be Phe^{177} in human and insect cell lines (17, 38). Our previous findings suggest that Ile^{176} and Phe^{177} of the HCV core protein may be responsible for SPP-dependent cleavage, because the replacement of Ile^{176} and Phe^{177} with Ala and Leu, respectively, abrogated intramembrane cleavage by SPP and impaired virus production (17, 28, 39). Weihofen et al. reported that SPP cleaved a peptide bond of the alpha-helix-breaking structure in a transmembrane region of the membrane protein (40). The replacement of Ile^{176} and Phe^{177} with Ala and Leu, respectively, in the HCV core protein converted the beta-sheet structure (alpha-helix-breaking structure) to an alpha-helix structure in the transmembrane region, as reported previously (28) (Fig. 6A and B). Ile^{190} and Phe^{191} of the EHcV core protein, which correspond to Ile^{176} and Phe^{177}, respectively, of the HCV core protein, reside in the alpha-helix-breaking structure of the transmembrane region (Fig. 6A and B). In contrast, the replacement of Ile^{190} and Phe^{191} with Ala and Leu, respectively, in the EHcV core protein were predicted to convert the beta-sheet to an alpha-helix structure in a manner similar to that for the HCV core protein (Fig. 6A and B). To investigate the involvement of SPP in the maturation of the EHcV core protein, we expressed EHcVc or HCVc in 293FT cells with an SPP or SPP mutant. These core proteins were expected to be resistant to signal peptidase-dependent processing because the C-terminal residue Ala of both core proteins was replaced with Arg, resulting in the detection of an immature core protein by the anti-HA antibody (Fig. 6A) (28). The core proteins with molecular masses of 23 kDa and 28 kDa were detected mainly with the anti-FLAG antibody in 293FT cells expressing HCVc and HCVc-mt, respectively (Fig. 6C, lanes 2 and 3); however, the 23-kDa band was not detected with the anti-HA antibody (Fig. 6C, lane 2). When EHcVc was expressed in 293FT cells, it was detected at a molecular mass of 27 kDa with the anti-FLAG antibody, but not with the anti-HA antibody (Fig. 6C, lane 4). In contrast, EHcV-mt, in which the 190th and 191st residues were Ala and Leu instead of Ile and Phe, respectively, was detected mainly at a molecular mass of 30 kDa with the anti-FLAG and anti-HA antibodies (Fig. 6C, lane 5). A loss-of-function SPP mutant (SPP-D219A) in which the 219th residue was Ala instead of Asp was shown to have a dominantly negative effect on SPP-dependent cleavage of the

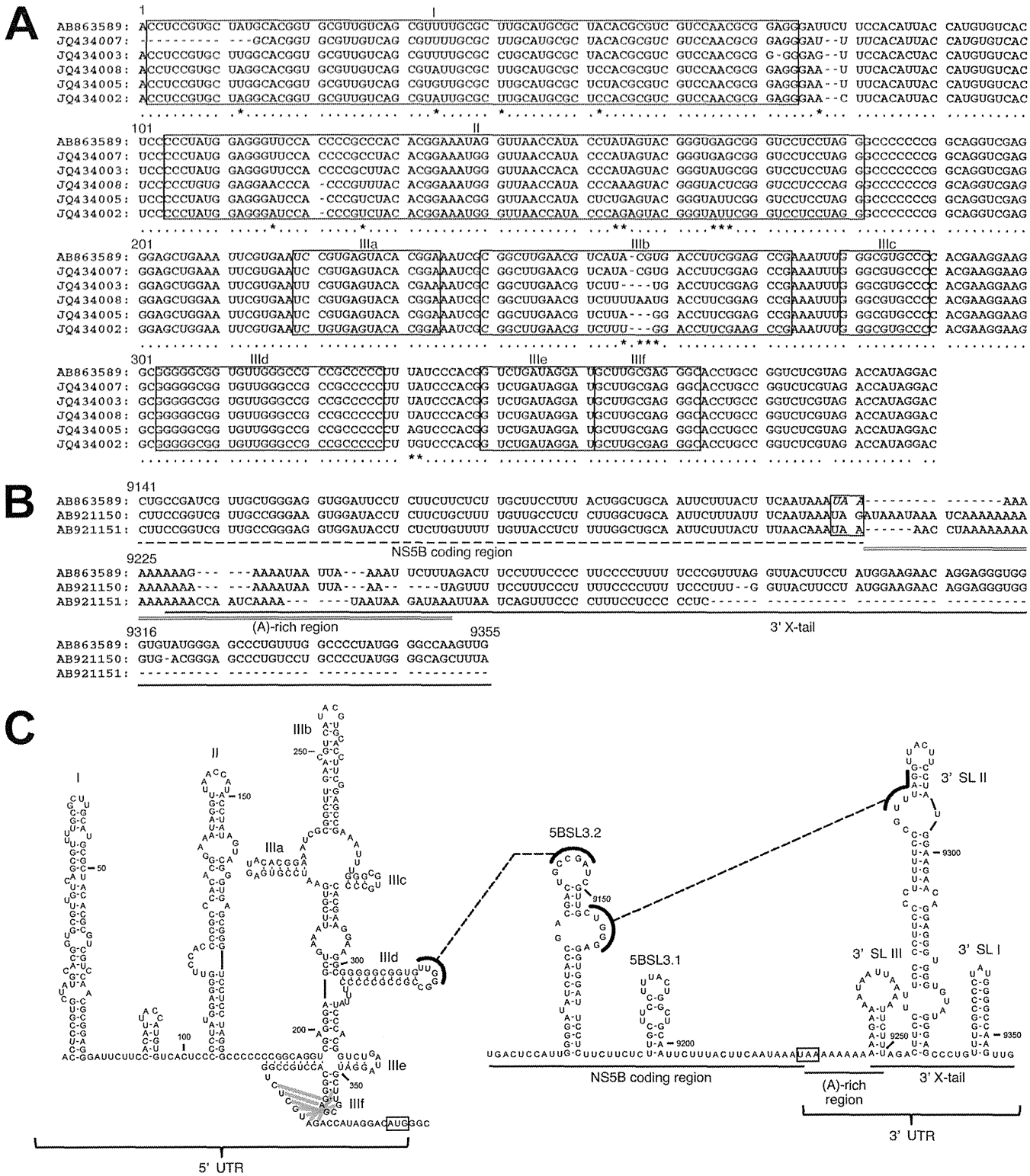

FIG 4 RNA structure analysis of the 5′ and 3′ ends of EHcV. (A) Alignment of the 5′ UTRs of the EHcV strains. Asterisks and black lines indicate variable residues and miRNA-targeting regions, respectively. SL structures are enclosed in rectangles. GenBank numbers are listed in the legend to Fig. 3. (B) Alignment of the 3′ UTRs of the EHcV strains. The 3′-terminal sequences with GenBank numbers AB921150 and AB921151 were determined using serum samples 5 and 1, respectively, and were aligned with that of JPN3/JAPAN/2013 (GenBank accession no. AB863589). (C) The secondary structures of the 5′ UTR, NS5B-coding region, and 3′ UTR were predicted on the basis of minimum free energy predictions. The stem loops in the 5′ UTR (left) were designated according to the stem loops of the HCV 5′-UTR structures (30). A gray line, double line, and single line indicate a pseudoknot structure, miR-122-target region, and complementary sequence, respectively. The stem loops in the NS5B-coding region and 3′ UTR (right) were designated to correspond to the stem loops embedded in the HCV 3′-terminal region (32, 33). The NS5B-coding region, (A)-rich region, and 3′-X-tail sequence are indicated under the schematic structure. Start and stop codons are enclosed by rectangles.

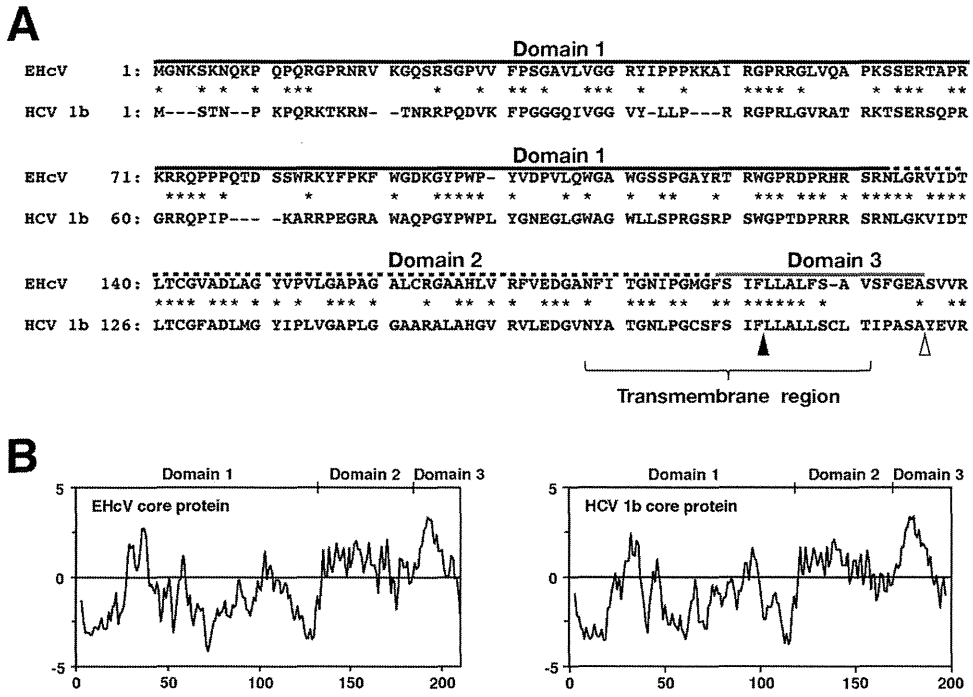

FIG 5 Amino acid alignment and hydrophobicity of EHcV and HCV core proteins. (A) Alignment of the core proteins of EHcV (JPN3/JAPAN/2013) and HCV genotype1b (Con1; GenBank accession number AJ238799). Asterisks indicate identical amino acid residues. Bars indicate gaps to achieve maximum amino acid matching. The black and white arrowheads indicate the predicted cleavage site of the core protein of HCV by SPP and signal peptidase, respectively. The EHcV core protein was composed of three domains, domain 1 (a black line, residues 2 to 132), domain 2 (a broken black line, residues 133 to 187), and domain 3 (a gray line, residues 188 to 204), relative to those of the HCV core protein (42). (B) Hydrophobicity plots of the EHcV and HCV core proteins were prepared by the method of Kyte and Doolittle (26). The horizontal and vertical axes represent amino acid position and hydrophobicity, respectively.

HCV core protein and to be coprecipitated with the immature core protein (28). HCVc had a molecular mass of 23 kDa in the presence of wild-type SPP (SPP-wt) and was detected with the anti-FLAG antibody, but not with the anti-HA antibody (Fig. 6D, lane 2), suggesting that the 23-kDa protein band may be a mature core protein. HCVc mainly had a molecular mass of 28 kDa in the presence of SPP-D219A and was detected with the anti-FLAG and anti-HA antibodies (Fig. 6D, lane 3), which corresponds to the mobility of HCVc-mt (Fig. 6D, lane 4). These results suggest that SPP-D219A may abrogate the intramembrane cleavage of HCVc. In a manner similar to that for the HCV core protein, EHcVc was detected mainly at a molecular mass of 27 kDa in the presence of SPP-wt with the anti-FLAG antibody, but not with the anti-HA antibody (Fig. 6D, lane 6). EHcVc was detected mainly at a molecular mass of 30 kDa in the presence of SPP-D219A with anti-FLAG and anti-HA antibodies (Fig. 6D, lane 7), corresponding to the mobility of EHcVc-mt (Fig. 6D, lane 8). When SPP-D219A was coexpressed with either HCVc or EHcVc, immature HCVc and EHcVc were coprecipitated with SPP-D219A (Fig. 6E, lanes 3 and 5). These results suggest that the EHcV core protein may be cleaved by SPP and that Ile^{190} and Phe^{191} of the EHcV core protein are critical for SPP-dependent cleavage.

The intracellular localization of the hepacivirus core protein. The HCV core protein is known to be localized mainly on the surface of LDs and is partially fractionated in the detergent-resistant membrane (DRM) close to the budding sites on the ER (13, 14, 16, 17). The core protein is considered to encompass the viral genome on the ER membrane, followed by budding into the lumen side (13, 14, 16, 17). To examine the intracellular localization of the EHcV core protein, we expressed HCVc or EHcVc in the Huh7OK1 cell line and stained the core proteins with the anti-FLAG antibody after staining LDs. Consistent with the findings of previous studies (14, 41, 42), HCVc was localized mainly on LDs (Fig. 7, row 3), whereas HCV-mt was not (Fig. 7, row 4). In a manner similar to that for the HCV core protein, EHcVc was localized mainly on LDs (Fig. 7, top row), whereas EHcVc-mt was not (Fig. 7, second row). These results suggest that the EHcV core protein may be localized mainly on LDs after SPP-dependent cleavage.

The DRM is defined as the cholesterol/sphingolipid-rich microdomain, which is resistant to nonionic detergents such as Triton X-100, considered to be a characteristic of lipid rafts. HCV was previously shown to be propagated in lipid raft-like compartments, including the membranous web (43–45). Furthermore, the HCV core protein is known to be associated with lipid raft-like compartments as well as LDs (16, 17, 41, 42). Therefore, we determined whether the EHcV core protein could be detected in the DRM fractions. EHcVc or EHcVc-mt was expressed in 293FT cells. The resulting cells were lysed on ice in the presence or absence of 1% Triton X-100. The DRM fractions were separated from the soluble proteins by a flotation assay with a stepwise density gradient in the presence or absence of Triton X-100. Serial fractions were collected after ultracentrifugation and were then subjected to Western blot analysis after being concentrated. EHcVc and EHcVc-mt were fractionated broadly from fractions of samples 3 to 11 without Triton X-100, and the fraction from

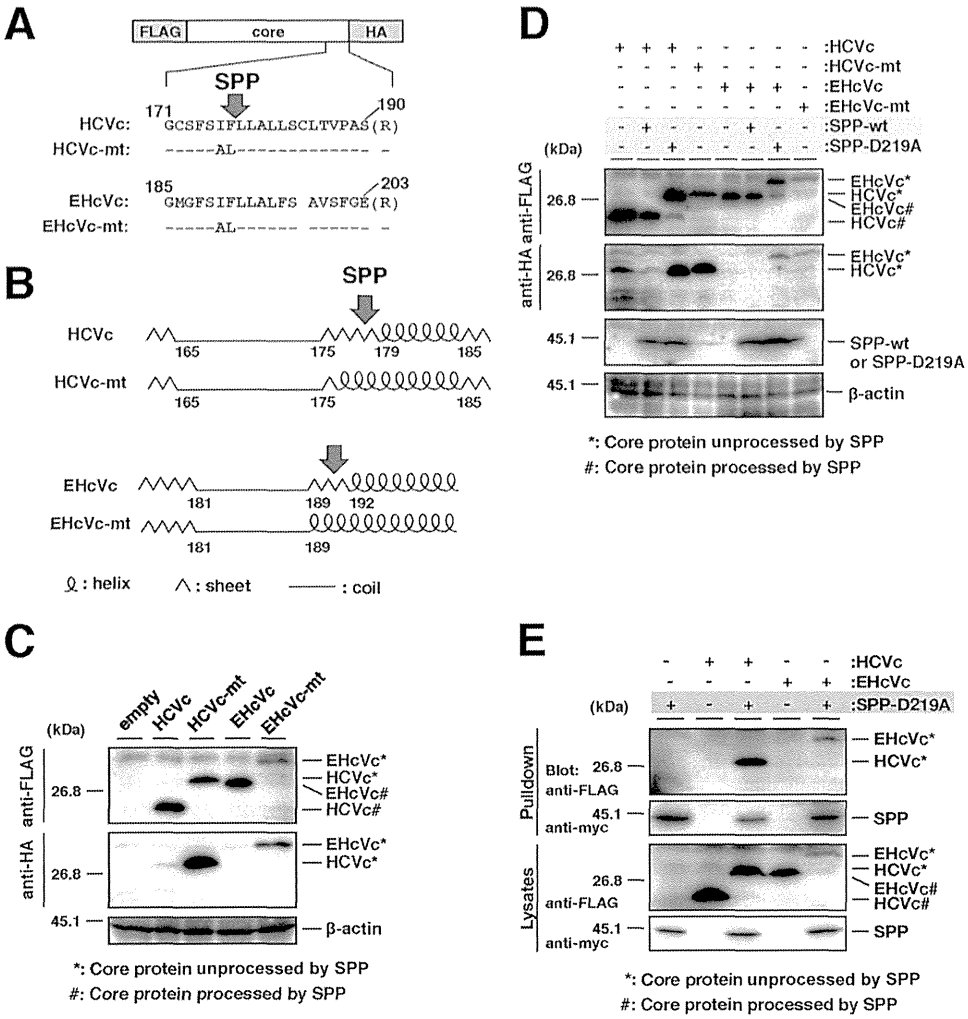

FIG 6 Intramembrane processing of the EHcV core protein by SPP. (A) The plasmids encoding HCVc, HCVc-mt, EHcVc, and EHcVc-mt are shown as a schematic diagram. Their C-terminal regions (171 to 190, HCV core protein; 185 to 203, EHcV core protein) were aligned. The C-terminal Ala of each core protein was replaced with Arg (R) to prevent signal peptidase-dependent cleavage for the detection of the SPP-uncleaved core protein with the anti-HA antibody. Bars indicate the amino acids that were the same as those of the wild-type residues. (B) The secondary protein structures in the C-terminal transmembrane regions of the HCV and EHcV core proteins and mutants were predicted by the method of Garnier et al. (25). Arrows indicate putative SPP cleavage sites. (C) HCVc, HCVc-mt, EHcVc, and EHcVc-mt were expressed in 293FT cells and immunoblotted with the anti-FLAG and -HA antibodies. (D) HCVc or EHcVc was expressed with SPP-wt or SPP-D219A in the 293FT cell line. HCVc-mt and EHcVc-mt were expressed in the absence of SPP-wt and SPP-D219A as uncleavable controls. (E) HCVc or EHcVc was coexpressed with or without SPP-D219A. SPP-D219A was pulled down with Ni beads. Coprecipitated proteins were immunoblotted with the anti-FLAG antibody.

sample 8 contained the largest amount of the core protein (Fig. 8, left panels). The distributions of the core proteins were roughly consistent with that of calreticulin, a marker protein of the ER membrane. When the cells expressing EHcVc were lysed in the presence of Triton X-100, a large amount of the core protein was localized in fractions 9 to 11 (Fig. 8, top three panels on the right). These fractions were enriched in calreticulin, corresponding to the detergent-soluble fractions (Fig. 8, fractions 7 to 11, top three panels on the right). However, EHcVc was partially detected in fractions 3 to 6 together with caveolin-1, a marker protein of the lipid raft (Fig. 8, fractions 3 to 6, top three panels on the right), suggesting that the EHcV core protein may have been partially distributed in the DRM fractions. In contrast, EHcVc-mt was localized in the detergent-soluble fractions (Fig. 8, fractions 9 to 11, bottom three panels on the right), but not in the DRM fractions (Fig. 8, fractions 3 to 6, bottom three panels on the right), in the presence of Triton X-100. EHcVc-mt was resistant to SPP-dependent processing, as described above (Fig. 6). These results suggest that the EHcV core protein may have been partially localized in the DRM and also that SPP-dependent processing may be required for DRM localization of the EHcV core protein.

DISCUSSION

The results of the present study indicate that EHcV infects Japanese-born domestic horses. Previous studies suggested that EHcV infected mainly horses and rarely dogs (5, 7–9). Our results demonstrate that EHcV commonly infects Japanese-born domestic horses (35.6% PCR positive and 22.6% seropositive). Several groups reported a prevalence of less than 10% PCR positivity in horses raised in the United States, the United Kingdom, and Ger-

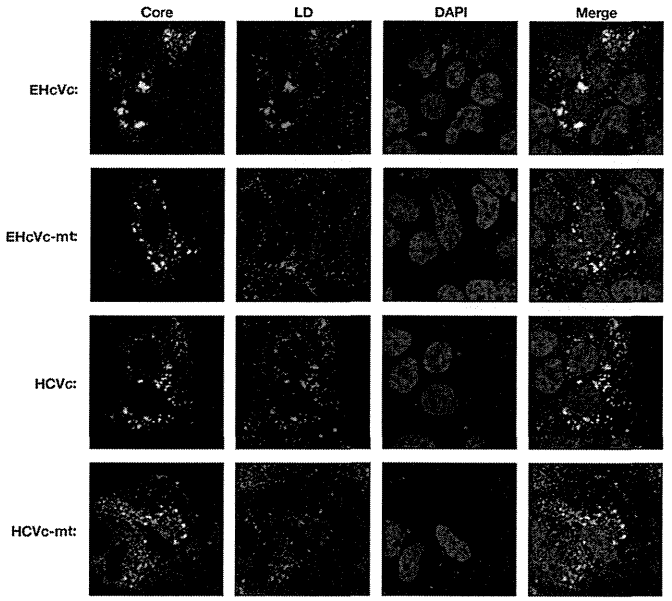

FIG 7 Intracellular localization of hepacivirus core proteins. HCVc, HCVc-mt, EHcVc, or EHcVc-mt was expressed in the Huh7OK1 cell line. The resulting cells were stained with Bodipy 558/568 (red) and then fixed with 4% paraformaldehyde at 24 h posttransfection, permeabilized, and subjected to indirect immunofluorescence staining. Each core protein was detected using mouse anti-FLAG antibodies and then Alexa 488-conjugated anti-mouse IgG (green). Cell nuclei were stained with DAPI after fixation (blue).

many (5, 7–9). Although the infection route of EHcV remains unknown, horses that were previously imported to Japan may be highly infected with EHcV. The serological prevalence in the present study appeared to be lower than that reported previously (8). A specific signal of the viral protein may be selected by Western blotting, used herein, rather than by the luciferase immunoprecipitation system, as reported previously (8), since the serum of each horse reacted to different proteins irrespective of the EHcV core protein (Fig. 2). The predicted full sequence of the EHcV strain amplified from serum sample 3 had high homology to those of the previously reported strains (Table 2). The polyproteins of previous strains had approximately 95% amino acid homology to one another irrespective of the area in which the horses originated, suggesting that these strains may belong to the same virological species. The parents of horse number 3 were born in Japan, while its grandparents were imported from the United States and Canada. Unfortunately, the sera of the parents and grandparents were not obtained in the present study. The EHcV strains obtained from Japanese-born horses may have originated from the United States or Canada. Another possibility is that one species of EHcV may have recently been distributed worldwide.

The primary and secondary structures of both UTRs are conserved among HCV strains and are essential for replication and translation. Four major stem-loop (SL) motifs have been detected in the 5′ UTR of the HCV genome, three SL structures of which are known to be required for IRES activity (46). Domain IIId plays a crucial role in anchoring of the 40S ribosome for IRES activity (47). Domain IIIb and the four-way helical junction of domains IIIa, IIIb, and IIIc bind eukaryotic initiation factor 3 (eIF3) and form a ternary complex, thereby forming the 48S preinitiation complex on HCV RNA (48). Moreover, domain II is known to be required to enhance eIF5-mediated GTP hydrolysis and the release of eIF2 from the 48S complex (48). These equivalent motifs were observed in the predicted secondary structures of the 5′ UTR of the reported EHcV strains (49), as well as in strain JPN3/JAPAN/2013 in the present study (Fig. 4C). A recent study demonstrated that the EHcV 5′ UTR exhibited IRES-dependent translation activity (50); however, further studies are needed to fully understand the IRES activity of the EHcV 5′UTR.

SL motifs embedded in the NS5B-coding region and UTRs of the HCV genome are known to be associated with viral replication. Several studies found that the mutational disruption of the complement sequence between 5BSL3.2 and 3′SL2 inhibited HCV RNA replication (33, 51). Additionally, the apical loop of domain IIId in the HCV 5′ UTR was shown to interact with the bulge of 5BSL3.2, supporting IRES-dependent translation and viral RNA replication (34–36). The RNA secondary structures of the 3′ UTR in the EHcV genome remained unknown due to limited information on its nucleotide sequence. 3′ RACE using poly(U) polymerase was employed in the present study because the ordinary 3′-RACE reaction using poly(A) polymerase was stopped at the (A)-rich region of the EHcV 3′ UTR. The nucleotide sequence of the EHcV 3′ UTR was determined, and its RNA secondary structure was then predicted (Fig. 4B and C). The results of the present

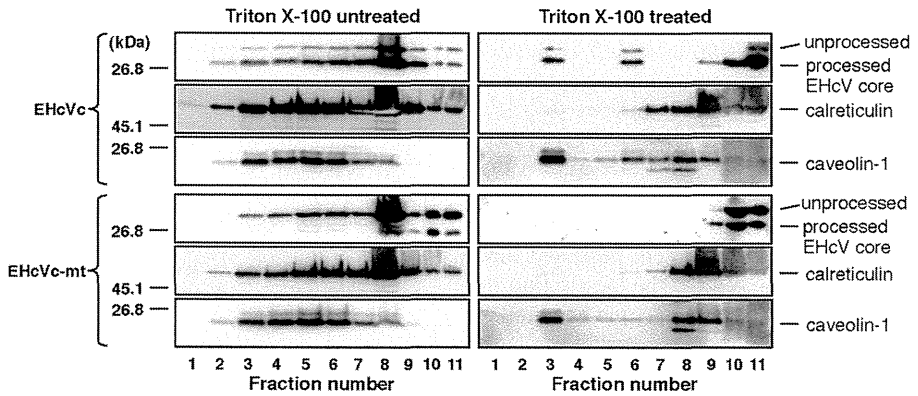

FIG 8 The EHcV core protein partially migrated to the DRM fraction after SPP-dependent processing. 293FT cells expressing either EHcVc or EHcVc-mt were homogenized with or without 1% Triton X-100 and then subjected to a flotation assay. Proteins in each fraction were concentrated with cold acetone and then subjected to Western blotting using the anti-FLAG, anti-calreticulin, or anti-caveolin-1 antibody.

study revealed that the 3′ UTR of the EHcV genome consists of the (A)-rich sequence and relatively shorter 3′-X-tail sequence. The three SL structures of the EHcV 3′ UTR were similar to those of the HCV 3′ UTR but were markedly different from the 3′ UTRs of GBV-B and rodent hepaciviruses. Drexler et al. described the structural characteristics of the 5′ and 3′ UTRs in rodent hepacivirus as well as phylogenetic information, liver tropism, and the pathogenicity of the virus (5). The SL motifs embedded in the 3′ X-tails of rodent hepacivirus and GBV-B varied. The structures of the 3′ UTRs appeared to correspond to the phylogenetic relationship of the hepaciviruses (5). Figure 4C shows that there were two stem-loop structures within the NS5B-coding region of EHcV corresponding to 5BSL3.2 and 5BSL3.3 of HCV RNA. Complementary regions were observed between the 5BSL3.2-like domain and 3′SL2, as well as between the 5BSL3.2-like domain and domain IIId of the EHcV genome (Fig. 4B and C). The kissing-loop and long-range RNA-RNA interactions may be structurally conserved between EHcV and HCV. Functional analyses of the *cis*-acting elements of the EHcV genome will contribute to the establishment of an EHcV infection system.

The mature HCV core protein was previously shown to be generated from the viral precursor polyprotein by signal peptidase followed by SPP-dependent processing of the transmembrane region (52). The core proteins of HCV and GBV-B are known to be cleaved by SPP (12, 37). The transmembrane regions of both the HCV and EHcV core proteins were found to be structurally conserved, based on their amino acid sequences and hydrophobicity plots (Fig. 5A and B and Fig. 6B). The replacement of Ile^{190} and Phe^{191} with Ala and Leu, respectively, in the EHcV core protein abrogated the intramembrane processing of the EHcV core protein (Fig. 6C). The loss-of-function mutant of SPP inhibited intramembrane processing of the EHcV core protein (Fig. 6D). Furthermore, the loss-of-function mutant of SPP specifically interacted with an uncleaved form of the EHcV core protein (Fig. 6E). These results indicate that the transmembrane region of the EHcV core protein may have been cleaved by SPP. The mature HCV core protein is known to be translocated into LDs and partially on lipid raft-like membranes. Previous studies reported that the HCV core protein on the LDs may be recruited near the replication complex in the membranous web, which consists of cholesterol- and sphingolipid-rich lipid components (43–45). Viral assembly was shown to occur on the ER membrane close to LDs and the membranous web (14). In addition to the HCV core protein, the nonstructural proteins and viral RNA of HCV were detected in the DRM fractions. The HCV RNA polymerase NS5B was previously reported to interact with sphingomyelin (53). Furthermore, a serine palmitoyltransferase inhibitor suppressed HCV replication by disrupting the replication complex (53, 54). These findings indicate that the DRM is provided as a scaffold for the formation of the HCV replication complex (45, 54). In the present study, we showed that the mature EHcV core protein was localized mainly on LDs and partially on the DRM (Fig. 7 and 8). A mutational analysis of the EHcV core protein indicated that SPP-dependent cleavage may be required for the localization of the EHcV core protein on LDs and the DRM in a manner similar to that for the HCV core protein. In addition, the assembly mechanism of EHcV may be similar to that of HCV.

In conclusion, the results of the present study show that EHcV shares common features with the HCV genomic structure and the biological properties of the capsid protein. *In vivo* and *ex vivo* infection systems for EHcV have not yet been successfully established. SCID mice carrying chimeric human livers are currently employed as a small animal model for *in vivo* infection with HCV (55) but are not suitable for studies on immunity and pathogenicity due to an immunodeficiency. Chimpanzees are not yet available for *in vivo* HCV research. Further studies on the mechanisms underlying EHcV infection will contribute to the development of an *in vivo* surrogate model system for studying HCV immunity and pathogenicity.

ACKNOWLEDGMENTS

We thank M. Furugori for her secretarial work, I. Katoh for helpful discussions, and C. Endoh for technical assistance.

This work was supported by Grants-in-Aid from the Ministry of Health, Labor, and Welfare, Japan (H24-Kanen-008 and H25-Kanen-002 and -008); the Ministry of Education, Culture, Sports, Science, and Technology, Japan; and the Japan Science and Technology Agency (JST) (Houga-24659204).

REFERENCES

1. **Simons JN, Leary TP, Dawson GJ, Pilot-Matias TJ, Muerhoff AS, Schlauder GG, Desai SM, Mushahwar IK.** 1995. Isolation of novel virus-like sequences associated with human hepatitis. Nat. Med. **1**:564–569. http://dx.doi.org/10.1038/nm0695-564.
2. **Beames B, Chavez D, Lanford RE.** 2001. GB virus B as a model for hepatitis C virus. ILAR J. **42**:152–160. http://dx.doi.org/10.1093/ilar.42.2.152.
3. **Bukh J, Apgar CL, Govindarajan S, Purcell RH.** 2001. Host range studies of GB virus-B hepatitis agent, the closest relative of hepatitis C virus, in New World monkeys and chimpanzees. J. Med. Virol. **65**:694–697. http://dx.doi.org/10.1002/jmv.2092.
4. **Quan PL, Firth C, Conte JM, Williams SH, Zambrana-Torrelio CM, Anthony SJ, Ellison JA, Gilbert AT, Kuzmin IV, Niezgoda M, Osinubi MO, Recuenco S, Markotter W, Breiman RF, Kalemba L, Malekani J, Lindblade KA, Rostal MK, Ojeda-Flores R, Suzan G, Davis LB, Blau DM, Ogunkoya AB, Alvarez Castillo DA, Moran D, Ngam S, Akaibe D, Agwanda B, Briese T, Epstein JH, Daszak P, Rupprecht CE, Holmes EC, Lipkin WI.** 2013. Bats are a major natural reservoir for hepaciviruses and pegiviruses. Proc. Natl. Acad. Sci. U. S. A. **110**:8194–8199. http://dx.doi.org/10.1073/pnas.1303037110.
5. **Drexler JF, Corman VM, Muller MA, Lukashev AN, Gmyl A, Coutard B, Adam A, Ritz D, Leijten LM, van Riel D, Kallies R, Klose SM, Gloza-Rausch F, Binger T, Annan A, Adu-Sarkodie Y, Oppong S, Bourgarel M, Rupp D, Hoffmann B, Schlegel M, Kummerer BM, Kruger DH, Schmidt-Chanasit J, Setien AA, Cottontail VM, Hemachudha T, Wacharapluesadee S, Osterrieder K, Bartenschlager R, Matthee S, Beer M, Kuiken T, Reusken C, Leroy EM, Ulrich RG, Drosten C.** 2013. Evidence for novel hepaciviruses in rodents. PLoS Pathog. **9**:e1003438. http://dx.doi.org/10.1371/journal.ppat.1003438.
6. **Kapoor A, Simmonds P, Scheel TK, Hjelle B, Cullen JM, Burbelo PD, Chauhan LV, Duraisamy R, Sanchez Leon M, Jain K, Vandegrift KJ, Calisher CH, Rice CM, Lipkin WI.** 2013. Identification of rodent homologs of hepatitis C virus and pegiviruses. mBio **4**(2):e00216–13. http://dx.doi.org/10.1128/mBio.00216-13.
7. **Lyons S, Kapoor A, Sharp C, Schneider BS, Wolfe ND, Culshaw G, Corcoran B, McGorum BC, Simmonds P.** 2012. Nonprimate hepaciviruses in domestic horses, United Kingdom. Emerg. Infect. Dis. **18**:1976–1982. http://dx.doi.org/10.3201/eid1812.120498.
8. **Burbelo PD, Dubovi EJ, Simmonds P, Medina JL, Henriquez JA, Mishra N, Wagner J, Tokarz R, Cullen JM, Iadarola MJ, Rice CM, Lipkin WI, Kapoor A.** 2012. Serology-enabled discovery of genetically diverse hepaciviruses in a new host. J. Virol. **86**:6171–6178. http://dx.doi.org/10.1128/JVI.00250-12.
9. **Kapoor A, Simmonds P, Gerold G, Qaisar N, Jain K, Henriquez JA, Firth C, Hirschberg DL, Rice CM, Shields S, Lipkin WI.** 2011. Characterization of a canine homolog of hepatitis C virus. Proc. Natl. Acad. Sci. U. S. A. **108**:11608–11613. http://dx.doi.org/10.1073/pnas.1101794108.
10. **van der Laan LJ, de Ruiter PE, van Gils IM, Fieten H, Spee B, Pan Q, Rothuizen J, Penning LC.** 5 June 2014. Canine hepacivirus and idiopathic

hepatitis in dogs from a Dutch cohort. J. Viral Hepat. http://dx.doi.org/10.1111/jvh.12268.
11. **Hüssy P, Langen H, Mous J, Jacobsen H.** 1996. Hepatitis C virus core protein: carboxy-terminal boundaries of two processed species suggest cleavage by a signal peptide peptidase. Virology **224:**93–104. http://dx.doi.org/10.1006/viro.1996.0510.
12. **Targett-Adams P, Schaller T, Hope G, Lanford RE, Lemon SM, Martin A, McLauchlan J.** 2006. Signal peptide peptidase cleavage of GB virus B core protein is required for productive infection in vivo. J. Biol. Chem. **281:**29221–29227. http://dx.doi.org/10.1074/jbc.M605373200.
13. **Hope RG, Murphy DJ, McLauchlan J.** 2002. The domains required to direct core proteins of hepatitis C virus and GB virus-B to lipid droplets share common features with plant oleosin proteins. J. Biol. Chem. **277:**4261–4270. http://dx.doi.org/10.1074/jbc.M108798200.
14. **Miyanari Y, Atsuzawa K, Usuda N, Watashi K, Hishiki T, Zayas M, Bartenschlager R, Wakita T, Hijikata M, Shimotohno K.** 2007. The lipid droplet is an important organelle for hepatitis C virus production. Nat. Cell Biol. **9:**1089–1097. http://dx.doi.org/10.1038/ncb1631.
15. **Samsa MM, Mondotte JA, Iglesias NG, Assuncao-Miranda I, Barbosa-Lima G, Da Poian AT, Bozza PT, Gamarnik AV.** 2009. Dengue virus capsid protein usurps lipid droplets for viral particle formation. PLoS Pathog. **5:**e1000632. http://dx.doi.org/10.1371/journal.ppat.1000632.
16. **Matto M, Rice CM, Aroeti B, Glenn JS.** 2004. Hepatitis C virus core protein associates with detergent-resistant membranes distinct from classical plasma membrane rafts. J. Virol. **78:**12047–12053. http://dx.doi.org/10.1128/JVI.78.21.12047-12053.2004.
17. **Okamoto K, Mori Y, Komoda Y, Okamoto T, Okochi M, Takeda M, Suzuki T, Moriishi K, Matsuura Y.** 2008. Intramembrane processing by signal peptide peptidase regulates the membrane localization of hepatitis C virus core protein and viral propagation. J. Virol. **82:**8349–8361. http://dx.doi.org/10.1128/JVI.00306-08.
18. **Aizaki H, Lee KJ, Sung VM, Ishiko H, Lai MM.** 2004. Characterization of the hepatitis C virus RNA replication complex associated with lipid rafts. Virology **324:**450–461. http://dx.doi.org/10.1016/j.virol.2004.03.034.
19. **Egger D, Wolk B, Gosert R, Bianchi L, Blum HE, Moradpour D, Bienz K.** 2002. Expression of hepatitis C virus proteins induces distinct membrane alterations including a candidate viral replication complex. J. Virol. **76:**5974–5984. http://dx.doi.org/10.1128/JVI.76.12.5974-5984.2002.
20. **Marchuk D, Drumm M, Saulino A, Collins FS.** 1991. Construction of T-vectors, a rapid and general system for direct cloning of unmodified PCR products. Nucleic Acids Res. **19:**1154. http://dx.doi.org/10.1093/nar/19.5.1154.
21. **Tajima S, Takasaki T, Matsuno S, Nakayama M, Kurane I.** 2005. Genetic characterization of Yokose virus, a flavivirus isolated from the bat in Japan. Virology **332:**38–44. http://dx.doi.org/10.1016/j.virol.2004.06.052.
22. **Tilgner M, Shi PY.** 2004. Structure and function of the 3′ terminal six nucleotides of the West Nile virus genome in viral replication. J. Virol. **78:**8159–8171. http://dx.doi.org/10.1128/JVI.78.15.8159-8171.2004.
23. **Saitou N, Nei M.** 1987. The neighbor-joining method: a new method for reconstructing phylogenetic trees. Mol. Biol. Evol. **4:**406–425.
24. **Tamura K, Peterson D, Peterson N, Stecher G, Nei M, Kumar S.** 2011. MEGA5: molecular evolutionary genetics analysis using maximum likelihood, evolutionary distance, and maximum parsimony methods. Mol. Biol. Evol. **28:**2731–2739. http://dx.doi.org/10.1093/molbev/msr121.
25. **Garnier J, Osguthorpe DJ, Robson B.** 1978. Analysis of the accuracy and implications of simple methods for predicting the secondary structure of globular proteins. J. Mol. Biol. **120:**97–120. http://dx.doi.org/10.1016/0022-2836(78)90297-8.
26. **Kyte J, Doolittle RF.** 1982. A simple method for displaying the hydropathic character of a protein. J. Mol. Biol. **157:**105–132. http://dx.doi.org/10.1016/0022-2836(82)90515-0.
27. **Zuker M.** 2003. Mfold web server for nucleic acid folding and hybridization prediction. Nucleic Acids Res. **31:**3406–3415. http://dx.doi.org/10.1093/nar/gkg595.
28. **Okamoto K, Moriishi K, Miyamura T, Matsuura Y.** 2004. Intramembrane proteolysis and endoplasmic reticulum retention of hepatitis C virus core protein. J. Virol. **78:**6370–6380. http://dx.doi.org/10.1128/JVI.78.12.6370-6380.2004.
29. **Okamoto T, Nishimura Y, Ichimura T, Suzuki K, Miyamura T, Suzuki T, Moriishi K, Matsuura Y.** 2006. Hepatitis C virus RNA replication is regulated by FKBP8 and Hsp90. EMBO J. **25:**5015–5025. http://dx.doi.org/10.1038/sj.emboj.7601367.
30. **Honda M, Brown EA, Lemon SM.** 1996. Stability of a stem-loop involving the initiator AUG controls the efficiency of internal initiation of translation on hepatitis C virus RNA. RNA **2:**955–968.
31. **Yanagi M, St Claire M, Emerson SU, Purcell RH, Bukh J.** 1999. In vivo analysis of the 3′ untranslated region of the hepatitis C virus after in vitro mutagenesis of an infectious cDNA clone. Proc. Natl. Acad. Sci. U. S. A. **96:**2291–2295. http://dx.doi.org/10.1073/pnas.96.5.2291.
32. **Blight KJ, Rice CM.** 1997. Secondary structure determination of the conserved 98-base sequence at the 3′ terminus of hepatitis C virus genome RNA. J. Virol. **71:**7345–7352.
33. **Friebe P, Boudet J, Simorre JP, Bartenschlager R.** 2005. Kissing-loop interaction in the 3′ end of the hepatitis C virus genome essential for RNA replication. J. Virol. **79:**380–392. http://dx.doi.org/10.1128/JVI.79.1.380-392.2005.
34. **Lourenço S, Costa F, Debarges B, Andrieu T, Cahour A.** 2008. Hepatitis C virus internal ribosome entry site-mediated translation is stimulated by cis-acting RNA elements and trans-acting viral factors. FEBS J. **275:**4179–4197. http://dx.doi.org/10.1111/j.1742-4658.2008.06566.x.
35. **Cristina J, del Pilar Moreno M, Moratorio G.** 2007. Hepatitis C virus genetic variability in patients undergoing antiviral therapy. Virus Res. **127:**185–194. http://dx.doi.org/10.1016/j.virusres.2007.02.023.
36. **Song Y, Friebe P, Tzima E, Junemann C, Bartenschlager R, Niepmann M.** 2006. The hepatitis C virus RNA 3′-untranslated region strongly enhances translation directed by the internal ribosome entry site. J. Virol. **80:**11579–11588. http://dx.doi.org/10.1128/JVI.00675-06.
37. **McLauchlan J, Lemberg MK, Hope G, Martoglio B.** 2002. Intramembrane proteolysis promotes trafficking of hepatitis C virus core protein to lipid droplets. EMBO J. **21:**3980–3988. http://dx.doi.org/10.1093/emboj/cdf414.
38. **Ogino T, Fukuda H, Imajoh-Ohmi S, Kohara M, Nomoto A.** 2004. Membrane binding properties and terminal residues of the mature hepatitis C virus capsid protein in insect cells. J. Virol. **78:**11766–11777. http://dx.doi.org/10.1128/JVI.78.21.11766-11777.2004.
39. **Kopp M, Murray CL, Jones CT, Rice CM.** 2010. Genetic analysis of the carboxy-terminal region of the hepatitis C virus core protein. J. Virol. **84:**1666–1673. http://dx.doi.org/10.1128/JVI.02043-09.
40. **Weihofen A, Binns K, Lemberg MK, Ashman K, Martoglio B.** 2002. Identification of signal peptide peptidase, a presenilin-type aspartic protease. Science **296:**2215–2218. http://dx.doi.org/10.1126/science.1070925.
41. **Barba G, Harper F, Harada T, Kohara M, Goulinet S, Matsuura Y, Eder G, Schaff Z, Chapman MJ, Miyamura T, Brechot C.** 1997. Hepatitis C virus core protein shows a cytoplasmic localization and associates to cellular lipid storage droplets. Proc. Natl. Acad. Sci. U. S. A. **94:**1200–1205. http://dx.doi.org/10.1073/pnas.94.4.1200.
42. **Hope RG, McLauchlan J.** 2000. Sequence motifs required for lipid droplet association and protein stability are unique to the hepatitis C virus core protein. J. Gen. Virol. **81:**1913–1925.
43. **Gao L, Aizaki H, He JW, Lai MM.** 2004. Interactions between viral nonstructural proteins and host protein hVAP-33 mediate the formation of hepatitis C virus RNA replication complex on lipid raft. J. Virol. **78:**3480–3488. http://dx.doi.org/10.1128/JVI.78.7.3480-3488.2004.
44. **Gosert R, Egger D, Lohmann V, Bartenschlager R, Blum HE, Bienz K, Moradpour D.** 2003. Identification of the hepatitis C virus RNA replication complex in Huh-7 cells harboring subgenomic replicons. J. Virol. **77:**5487–5492. http://dx.doi.org/10.1128/JVI.77.9.5487-5492.2003.
45. **Shi ST, Lee KJ, Aizaki H, Hwang SB, Lai MM.** 2003. Hepatitis C virus RNA replication occurs on a detergent-resistant membrane that cofractionates with caveolin-2. J. Virol. **77:**4160–4168. http://dx.doi.org/10.1128/JVI.77.7.4160-4168.2003.
46. **Tsukiyama-Kohara K, Iizuka N, Kohara M, Nomoto A.** 1992. Internal ribosome entry site within hepatitis C virus RNA. J. Virol. **66:**1476–1483.
47. **Babaylova E, Graifer D, Malygin A, Stahl J, Shatsky I, Karpova G.** 2009. Positioning of subdomain IIId and apical loop of domain II of the hepatitis C IRES on the human 40S ribosome. Nucleic Acids Res. **37:**1141–1151. http://dx.doi.org/10.1093/nar/gkn1026.
48. **Kieft JS, Zhou K, Grech A, Jubin R, Doudna JA.** 2002. Crystal structure of an RNA tertiary domain essential to HCV IRES-mediated translation initiation. Nat. Struct. Biol. **9:**370–374. http://dx.doi.org/10.1038/nsb781.
49. **Locker N, Easton LE, Lukavsky PJ.** 2007. HCV and CSFV IRES domain II mediate eIF2 release during 80S ribosome assembly. EMBO J. **26:**795–805. http://dx.doi.org/10.1038/sj.emboj.7601549.

50. Stewart H, Walter C, Jones D, Lyons S, Simmonds P, Harris M. 2013. The non-primate hepacivirus 5′ untranslated region possesses internal ribosomal entry site activity. J. Gen. Virol. 94:2657–2663. http://dx.doi.org/10.1099/vir.0.055764-0.
51. Diviney S, Tuplin A, Struthers M, Armstrong V, Elliott RM, Simmonds P, Evans DJ. 2008. A hepatitis C virus *cis*-acting replication element forms a long-range RNA-RNA interaction with upstream RNA sequences in NS5B. J. Virol. 82:9008–9022. http://dx.doi.org/10.1128/JVI.02326-07.
52. Penin F, Dubuisson J, Rey FA, Moradpour D, Pawlotsky JM. 2004. Structural biology of hepatitis C virus. Hepatology 39:5–19. http://dx.doi.org/10.1002/hep.20032.
53. Hirata Y, Ikeda K, Sudoh M, Tokunaga Y, Suzuki A, Weng L, Ohta M, Tobita Y, Okano K, Ozeki K, Kawasaki K, Tsukuda T, Katsume A, Aoki Y, Umehara T, Sekiguchi S, Toyoda T, Shimotohno K, Soga T, Nishijima M, Taguchi R, Kohara M. 2012. Self-enhancement of hepatitis C virus replication by promotion of specific sphingolipid biosynthesis. PLoS Pathog. 8:e1002860. http://dx.doi.org/10.1371/journal.ppat.1002860.
54. Katsume A, Tokunaga Y, Hirata Y, Munakata T, Saito M, Hayashi H, Okamoto K, Ohmori Y, Kusanagi I, Fujiwara S, Tsukuda T, Aoki Y, Klumpp K, Tsukiyama-Kohara K, El-Gohary A, Sudoh M, Kohara M. 2013. A serine palmitoyltransferase inhibitor blocks hepatitis C virus replication in human hepatocytes. Gastroenterology 145:865–873. http://dx.doi.org/10.1053/j.gastro.2013.06.012.
55. Mercer DF, Schiller DE, Elliott JF, Douglas DN, Hao C, Rinfret A, Addison WR, Fischer KP, Churchill TA, Lakey JR, Tyrrell DL, Kneteman NM. 2001. Hepatitis C virus replication in mice with chimeric human livers. Nat. Med. 7:927–933. http://dx.doi.org/10.1038/90968.

EFdA, a Reverse Transcriptase Inhibitor, Potently Blocks HIV-1 *Ex Vivo* Infection of Langerhans Cells within Epithelium

Journal of Investigative Dermatology advance online publication, 2 January 2014; doi:10.1038/jid.2013.467

TO THE EDITOR

Despite increasing access to antiretroviral drugs, sexual transmission of HIV-1 remains a significant public health threat. A recent clinical trial, CAPRISA 004, of a vaginally administered microbicide using a nucleoside reverse transcriptase inhibitor (NRTI), tenofovir (TDF), has demonstrated that 1% TDF gel reduced HIV-1 acquisition by an estimated 39% overall (Abdool Karim *et al.*, 2010), indicating a potential utility of NRTI-based microbicides. In the VOICE study, however, a once-daily dosing regimen with TDF gel failed to demonstrate protective effects in at-risk women. These studies demonstrate the need to develop additional more potent microbicide candidates to potentially increase the activity to protect women from HIV-1 transmission.

We previously reported that a series of 4′-substituted NRTIs have excellent antiviral properties (Ohrui, 2006), and through optimization of such 4′-substituted NRTIs, 4′-ethynyl-2-fluoro-2′-deoxyadenosine (EFdA) was found to exert extremely potent activity against a wide spectrum of HIV-1 strains including highly multidrug-resistant clinical HIV-1 isolates, with favorable *in vitro* cell toxicities (Nakata *et al.*, 2007; Ohrui *et al.*, 2007). EFdA inhibited HIV-1 replication in activated peripheral blood mononuclear cells with an EC_{50} of 0.05 nM, a potency several orders of magnitude greater than any of the current clinically available NRTIs (Michailidis *et al.*, 2009). As the prevalence of new infections with drug-resistant HIV-1 variants could increase in the coming years (Nichols *et al.*, 2011), EFdA may be useful as a topical microbicide.

Langerhans cells (LCs) are dendritic cells located, among other sites, within genital skin and mucosal epithelium (Lederman *et al.*, 2006). In female rhesus macaques exposed intravaginally to simian immunodeficiency virus, up to 90% of initially infected target cells were LCs (Hu *et al.*, 2000). *Ex vivo* experiments with human foreskin explants show that epidermal LCs in inner foreskin are primary target cells for HIV-1 infection, providing a plausible explanation for why circumcision greatly reduces the probability of acquiring HIV-1 (Ganor *et al.*, 2010; Zhou *et al.*, 2011). LCs also express CD4 and CCR5, but not CXCR4, and demonstrate the distinctive characteristics of emigrating from tissue to draining lymph nodes in order to interact with T cells following contact with pathogens (Lederman *et al.*, 2006). Indeed, epidermal LCs are readily infected *ex vivo* with R5-HIV-1, but not with X4-HIV-1, and initiate and promote high levels of infection upon interactions with cocultured $CD4^+$ T cells (Kawamura *et al.*, 2000; Ogawa *et al.*, 2009, 2013), consistent with previous epidemiologic observations that the majority of HIV-1 strains isolated from newly infected patients are R5-HIV-1 strains (Zhu *et al.*, 1993). Thus, LCs likely have an important role in disseminating HIV-1 soon after exposure to the virus.

To understand how HIV-1 traverses skin and genital mucosa, an *ex vivo* model was developed in which resident LCs within epithelial tissue explants obtained from suction blisters are exposed to HIV-1 and then allowed to emigrate from the tissue, thus mimicking conditions that occur following mucosal exposure to HIV (Kawamura *et al.*, 2000; Ogawa *et al.*, 2009, 2013). In this model, although relatively few productively infected LCs are identified, these cells induce high levels of HIV-1 infection when cocultured with resting autologous $CD4^+$ T cells (Kawamura *et al.*, 2000; Ogawa *et al.*, 2013). As expected, when epidermal tissue explants were pretreated with various concentrations of TDF, EFdA, and CCR5 inhibitor, maraviroc (MVC), prior to R5-tropic HIV-$1_{Ba\text{-}L}$ exposure, HIV-1 infection of resident LCs within epidermis as well as subsequent virus transmission from emigrated LCs to cocultured $CD4^+$ T cells was decreased in a dose-dependent manner (Figure 1a and c; for detailed methods, see Supplementary Material). The blocking was confirmed by repeated experiments using skin explants from three additional randomly selected individuals (Figure 1b and d). Strikingly, although the blocking efficiency of TDF or MVC even at 5,000 nM was partial, EFdA demonstrated complete blocking of R5-HIV-1 replication in LCs as well as subsequent virus transmission from emigrated LCs to $CD4^+$ T cells at doses of 100–5,000 nM (Figure 1a–d). Furthermore, EFdA blocked *ex vivo* virus infection of LCs as well as subsequent virus transmission when two strains of R5-HIV-1, HIV-$1_{JR\text{-}FL}$ and HIV-1_{AD8}, were utilized in experiments ($n=3$, Supplementary Figure S1 online).

Similar to the results in epidermal LCs, preincubation of monocyte-derived LCs (mLCs) with 100–5,000 nM of EFdA

Abbreviations: EFdA, 4′-ethynyl-2-fluoro-2′-deoxyadenosine; LC, Langerhans cell; mLC, monocyte-derived LC; MVC, maraviroc; NRTI, nucleoside reverse transcriptase inhibitor; TDF, tenofovir

Accepted article preview online 11 November 2013

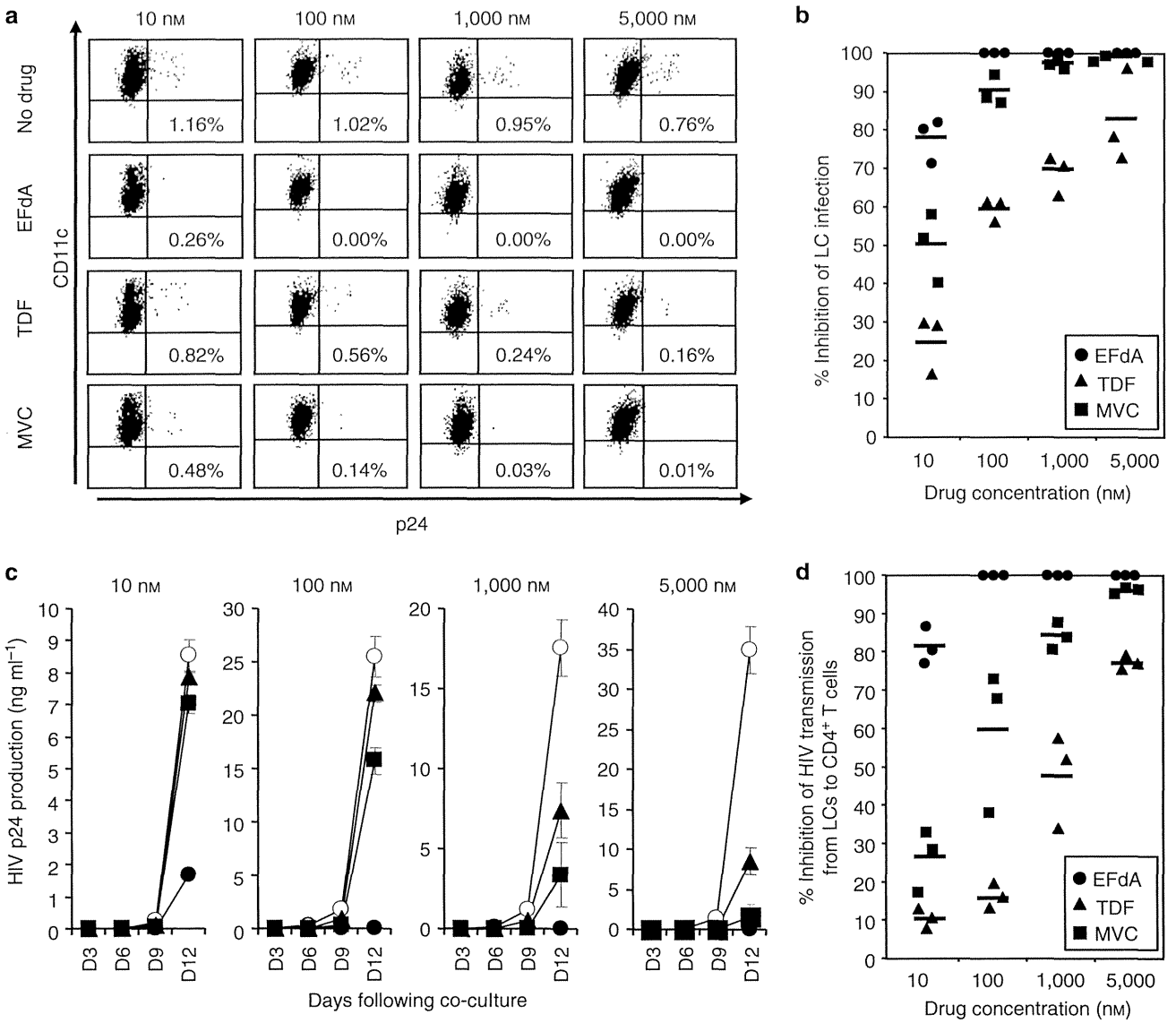

Figure 1. Preincubation of skin explants with EFdA blocks R5-HIV-1 infection in LCs and subsequent virus transmission to cocultured CD4$^+$ T cells. LCs within skin explants were preincubated with no drug (○) or the indicated concentrations of EFdA (●), TDF (▲), and MVC (■) for 30 minutes, exposed to HIV-1_{Ba-L} for 2 hours, and then floated on culture medium to allow migration of LCs from the explants. Emigrating cells from the epidermal sheets were collected 3 days following HIV-1 exposure. HIV-1-infected LCs were assessed by HIV-1 p24 intracellular staining in langerin$^+$ CD11c$^+$ LCs (**a**, **b**), or further cocultured with autologous CD4$^+$ T cells and culture supernatants were assessed for p24 content by ELISA on the indicated days (**c**, **d**). Summary of percent inhibition of LC infection (**b**) and virus transmission to CD4$^+$ T cells (**d**) of 12 experiments using skin explants from 12 individuals with the indicated each concentration of EFdA (●), TDF (▲), and MVC (■) are shown. Mean values obtained from different donors are shown as horizontal marks (**b**, **d**). EFdA, 4′-ethynyl-2-fluoro-2′-deoxyadenosine; LCs, Langerhans cells; MVC, maraviroc; TDF, tenofovir.

completely blocked HIV-1 replication in mLCs as well as subsequent virus transmission from mLCs to cocultured CD4$^+$ T cells, whereas both TDF and MVC at the same doses only partially inhibited the transmission (Figure 2a and b; for detailed methods, see Supplementary Material online). Intriguingly, even in 1–3 days following the removal of EFdA (1,000 nM), EFdA completely blocked HIV-1 infection of mLCs as well as subsequent virus transmission from mLCs to cocultured CD4$^+$ T cells, whereas TDF and MVC rapidly lost their anti-HIV-1 activity within days (Figure 2c–f). No cellular toxicity was noted for any of these drugs at the doses used in these experiments (Supplementary Figure S2 online). When similar experiments were conducted using peripheral blood mononuclear cell as target cells, virtually identical favorable persistency of EFdA in antiviral activity compared with that of TDF was observed (data not shown).

In the present work, we demonstrated that EFdA exerted extremely more potent anti-HIV-1 activity in LCs than did TDF and MVC, and the potent anti-HIV-1 activity of EFdA persisted for at least 3 days. Of note, the efficacy of TDF gel in CAPRISA 004 has been linked to its long intracellular half-life (Abdool Karim *et al.*, 2010; Rohan *et al.*, 2010). Our data strongly